Hardened AAM Properties

Patricia Kara De Maeijer, Kruthi Kiran Ramagiri, Mladena Lukovic, Laura Rossi, Giulia Masi, Arkamitra Kar, Pujitha Ganapathi Chottemada, Juho Yliniemi, Kazuo Ichimiya, Wei Sha, Frank Dehn, and Guang Ye

Abstract The introduction of alkali-activated concrete (AAC) technology to the construction industry represents a significant step toward a sustainable development and a cleaner environment by reducing environmental pollution. Currently, its application is relatively limited compared to traditional Portland cement based concrete (PCC). However, AAC has a remarkable potential for future growth and innovation despite several associated challenges and limitations. The current Chapter highlights recent progress in AAC mix design and its mechanical properties, paving the way

P. Kara De Maeijer (✉)
Faculty of Civil and Mechanical Engineering, Riga Technical University, Riga LV-1048, Latvia
e-mail: pkdm.rtu@gmail.com

Faculty of Applied Engineering, University of Antwerp, Antwerp 2020, Belgium

K. K. Ramagiri
MYK Laticrete, Hyderabad 502 329, Telangana, India

M. Lukovic
Department Engineering Structures, Faculty of Civil Engineering and Geosciences, Delft University of Technology, Delft 2628 CN, The Netherlands

L. Rossi · F. Dehn
Institute of Concrete Structures and Building Materials (IMB), Karlsruhe Institute of Technology (KIT), Karlsruhe DE-76131, Germany

G. Masi
Department of Civil, Chemical, Environmental and Materials Engineering, University of Bologna, Bologna 40131, Italy

A. Kar · P. Ganapathi Chottemada
Department of Civil Engineering, Birla Institute of Technology and Science-Pilani, Hyderabad 500 078, Telangana, India

J. Yliniemi
Fibre and Particle Engineering Research Unit, University of Oulu, Oulu FI-90014, Finland

K. Ichimiya
Department of Civil and Environmental Engineering, National Institute of Technology, Oita College, Oita 870-0152, Japan

W. Sha
School of Natural and Built Environment, Queen's University Belfast, Belfast BT9 5AG, UK

G. Ye and F. Dehn (eds.), *Mechanical Properties of Alkali-Activated Materials*, RILEM State-of-the-Art Reports 46, https://doi.org/10.1007/978-3-032-07116-3_7

for a broader application. The universally recognized international standards and codes for AAC, its mix design and evaluation of its long-term performance are still emerging. Unlike conventional PCC, AAC encompasses a wide class of materials with wide varying chemical composition and reaction mechanisms, depending on the choice of constituent materials (precursors and alkali activators). The mechanical properties, while diverse, reflect the flexibility of the material in response to different compositions and curing conditions. Though, non-uniformity makes consistent AAC usage challenging on the scale of PCC. Nevertheless, ongoing research and development efforts by RILEM TC 294-MPA are dedicated to tackling these challenges and enhancing the efficacy and widespread adoption of AAC technology.

Keywords Alkali-activated concrete (AAC) · Compressive strength · Flexural strength · Splitting tensile strength · Elastic modulus

1 Introduction

The continued research and development of alkali-activated concrete (AAC) technology, as well as its potential applications in sustainable and innovative construction projects, suggest its significance and expanding presence within the concrete industry in the future.

Various emerging trends and developments may impact its trajectory and use in the forthcoming years. One of the trends is the increased focus on sustainable, low-carbon or even net-zero building materials, driven by growing concerns over climate change. AAC is a promising option in this regard, as it can use alkali-activated binders (AABs) derived from industrial and municipal solid waste incineration by-products such as fly ash (FA), bottom ash (BA) and ground granulated blast furnace slag (GGBFS) as raw materials, thereby reducing the need for virgin materials and decreasing the carbon footprint associated with Portland cement (PC) and concrete production. Alkali-activated binders (AABs) have gained attention for their environmental sustainability, which has been supported by life cycle assessment (LCA) studies. Another trend is the continued development of novel alkali activators and pozzolanic materials, which could improve the performance and durability of AAC structures. In addition, the rapid setting properties of AAC increase interest in the use for precast and modular construction, presenting opportunities for accelerated project timeframes and cost effectiveness, while also improving quality and consistency. AAC is also being explored for use in high-performance applications, like bridges and pavements, where its inherent durability and resistance to chemical deterioration could be advantageous.

G. Ye
Section Materials and Environment, Department of 3MD, Faculty of Civil Engineering and Geosciences, Delft University of Technology, Delft 2628 CN, The Netherlands

2 State-of-the-Art Review

2.1 Alkali-Activated Materials (AAMs)

In the broadest classification, alkali-activated materials (AAMs) encompass essentially any binder system derived by the reaction of an alkali metal source (solid or dissolved) with a solid silicate-rich powder [1, 2]. This solid is typically an aluminosilicate precursor often containing varying amounts of additional chemical elements, such as calcium (Ca), aluminium (Al), and iron (Fe) exemplified by materials like GGBFS, natural pozzolan, FA, or BA [3]. AAMs are synthesized through the reaction of an aluminosilicate-based precursor (denoted as $xSiO_2 \cdot yAl_2O_3$), alkali activators (comprising MOH and M_2SiO_3; where M is either alkali ion Na^+ or K^+), and water (H_2O) [4]. The generally accepted classification of AAMs based on the chemical composition of the precursor is illustrated in Fig. 1.

The main function of the activator is to raise the pH of the reaction mix, thereby initiating the dissolution of the solid precursor. Alkali hydroxides and silicates are commonly used activators due to their high reactivity and chemical resistance [5, 6]. They provide good resistance to sulfates, acids (except very strong ones), and chlorides, while also improving short-term mechanical performance. However, their long-term impact on mechanical properties, volume stability and durability remain uncertain. Alkali carbonates (e.g. sodium carbonate, Na_2CO_3) may provide better long-term durability [7], considering that their moderate reaction rate promotes the formation of a denser and more stable microstructure, and reducing the risks of shrinkage, alkali-silica reaction (ASR), leaching, efflorescence, and carbonation.

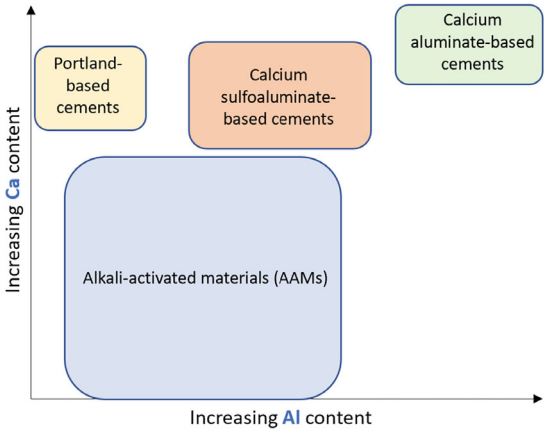

Fig. 1 Classification of AAMs [3]

2.2 Perspectives and Barriers in the Application of AAMs

Two patented sources could be mentioned as ground-breaking developments in the production of AAMs dated back to 1895 in the United States [8] and 1908 in Germany [9]. Subsequently, during the following years, production activities mainly centered in the former Soviet Union [10] and China [11], where cement shortages necessitated alternative materials search. In response, alkali activation was developed in both regions as a solution for overcoming this problem by using locally available materials and by-products, specifically GGBFS.

The fundamental research on AAMs has blossomed internationally only from the 1990s onwards. The early research works were focused on microstructure and mechanical properties of AAMs, with little emphasis on sustainability, prediction of service life, durability, and engineering properties [3, 12–15].

AAMs are recognized as potential alternatives to PC and blended cements such as CEM III/B (which contain 66–80% GGBFS and 20–34% clinker), offering possibilities to mitigate CO_2 emissions, improve durability and performance of concrete infrastructure, particularly in aggressive environments, and repurpose several by-products into useful products. AAMs based on FA and GGBFS blending often outperform CEM III/B in terms of mechanical strength gain, chemical resistance and thermal resistance. However, the alkali-activation process involves concentrated aqueous alkali solutions, which are corrosive, viscous, and, as such, difficult to handle and are unsuitable for user-friendly application, particularly on-site [16].

The key barriers hindering the industrial-scale production of AAMs lie beyond the direct technical realm. These include the need to control the entire supply chain, including reliance on alkali suppliers who have not been historically connected with applications in the construction industry. Moreover, existing competition, for some precursor materials with established usage in blended PC, complicates the adoption of AAMs [17].

In most cases, despite the occasional demonstrative application of AAMs in regions such as Australia, Europe and China, predictable performance can be achieved only after a tremendous amount of trial-and-error laboratory experimentation. That, in fact, limits the structural investigation of AACs in the field to proceed to widespread industrial implementation and application [18]. Nonetheless, AAC starts to gain traction within the construction industry. Over the past decade, several products based on alkali-activated technology have been available on the market [19], some of them are listed in Table 1.

The use of AAC is still relatively limited compared to traditional concrete, owing to several challenges and limitations associated with its use. Some of the main problems that have been identified include the following:

- *Uncertainty and non-applicability of existing codes and guidelines*: the absence of universally recognized standards or codes for AAC complicates its specification, mix design, and performance evaluation, leading to difficulties in the development of consistent production methods and making accurate performance predictions. The existing codes applied for PCC, which base design on compressive strength

Table 1 Example of AAC products available on the market

Product name	Company	Country	Description	References
E-crete	Zeobond Pty Ltd.	AUS	GGBFS + pulverized fuel ash (PFA)	[20]
Alkali-activated cement	ANSTO	AUS	Industrial glass and sand waste	[21]
	EXEGY Soletanche Bachy	FR	GGBFS + sodium carbonate	[22]
RAMAC	SQAPE BV	NL	Ready-mix cement free concrete	[23]
Porous AAC constructive blocks	ACCIONA	SP	FA	[24]
CEMFREE	DB Group	UK	GGBFS + PFA	[25]
Vertua® Ultra	CEMEX	UK	AAC	[26]
BlockwallsTM	Virtual Concrete Solutions Ltd.	UK	Precast AAC blocks	[27]

at 28 days, may not fully address the properties of AAC. For PCC, compressive strength at later ages remains constant or increases, and other mechanical properties are typically estimated based on this strength. However, it remains uncertain whether the same relations and assumptions are valid for AAC. In general, there is a lack of a straightforward mix design method for AAC that ensures a guaranteed compressive strength, therefore the development of tailored guidelines is crucial. While national regulations and specifications are available in Australia (VicRoads specifications—Section 703) [28], China (GB/T 29423–2012) [29], India (IS 17452:2020) [30], Switzerland (SIA Merkblatt 2049:2014) [31], Ukraine (DSTU B.V. 2.7-181:2009) [32] and UK (BSI Flex 350 v2.0:2024-09, BSI PAS 8820:2016) [33, 34], these may not fully address unique properties of AAC worldwide.

- *Lack of knowledge on long-term properties*: the investigation into the long-term mechanical properties' development of AAC remains sparce, with most studies focusing only on the mechanical properties up to 28 days. Consequently, there is no certainty regarding the mechanical properties' development of AAC over the long-term performance. It remains unclear whether the compressive strength at 28 days can be used as a reliable reference for design purposes. Reports indicate a decrease in compressive strength [35–37] or stiffness [38–41] over time for GGBFS-based and binary FA/GGBFS-based AACs. Though, it must be noted that these studies were performed with relatively small number of specimens to have proof of the mechanism. While AAC can offer improved durability compared to PCC in some cases (e.g., fire resistance, chemical resistance), there are still concerns about its long-term durability and resistance to various types of damage, such as freeze-thaw cycles, carbonation, creep, shrinkage, sulfate attack, acid attack and ASR. Prolonged drying of AAC, when it is exposed to moderate

humidity and air circulation conditions that lead to the evaporation of moisture, can impair the long-term durability and mechanical performance of AAC, particularly its stiffness and load-bearing capacity. This is influenced by the pore size distribution, packing density of the gel phases and volume stability characteristics like shrinkage and creep. These coupled effects play a critical role in determining the overall structural integrity of AAC under constant drying conditions, impacting both its microstructure and macroscopic behaviour.

- *High variation in raw materials properties*: AAC is far from a one-size-fits-all solution, as a wide range of precursors and activators are available, and the selection depends upon availability, reactivity, cost and environmental considerations [17]. This non-uniformity introduces challenges in achieving consistent results when using AAC, in particular on a scale comparable to PCC.
- *High variability in mechanical properties*: mechanical properties attributed to AAC, reported in the literature, vary significantly, depending on mix composition and curing conditions.
- *Limited availability of raw materials*: the availability and quality of the pozzolanic materials used in AAC can vary, thereby bringing an impact on the performance and consistency of the AAC. Moreover, a significant proportion of the total GGBFS is already being extensively used as a supplementary cementitious material (SCM) in blended PC, thereby limiting its availability for AAC production.
- *Higher cost*: the use of AAC can be more expensive compared to PCC due to the cost of the raw materials and the need for specialized equipment and curing conditions. However, the construction sector is often encouraged to adopt greener alternatives under environmental regulations, even when these options involve higher upfront costs. This shift is a part of a broader decarbonization trend, with governments implementing financial incentives like carbon taxes and pollution permits to promote sustainability. In fact, AAC could become more cost-effective than PCC, depending on the performance needs. As was mentioned above, AAC can easily achieve high strength and chemical resistance, while PCC may require thicker elements for similar functionality.
- *Limited knowledge and experience*: Unlike the standardized production processes of PCC, AAC lacks a straightforward production flowsheet due to complexity arising from the variability in its material composition, as different precursors and activators result in diverse chemical and mechanical properties. That leads to complicated development of consistent production methods and performance predictions for AAC. The commercialization and widespread application of AACs are still limited [42–45]. To facilitate the transition from laboratory research to commercially available construction material, research efforts should prioritize the investigation of material behaviour and long-term performance over the reaction process and short-term performance [46, 47]. That can definitely accelerate the adoption of AAC as an alternative in the construction sector.

Overall, while there are several challenges and limitations associated with the use of AAC, ongoing research and development efforts are actively focused on addressing

these issues. These efforts aim to improve the performance and acceptance of this technology over time.

2.3 Alkali-Activated Binders (AABs)

AABs can be formulated using two main methods: one-part AABs and two-part AABs. One-part AABs are produced by dry mixing of solid aluminosilicates with solid alkali activators, such as alkali hydroxides, silicates, sulfates or carbonates, with the addition of water, which is similar to PCC production process. Conversely, two-part AABs involve an activation of solid calcium-aluminosilicate precursors, such as FA, metakaolin (MK), or GGBFS, with aqueous sodium or potassium silicate solutions [16]. The one-part AABs offers easier handling by avoiding the use of hazardous liquid alkali solutions used in two-part AABs. In one-part AABs, all dry ingredients, including precursor and solid activator, are uniformly mixed before gradually adding water while stirring at low speed. In two-part AABs, the liquid activator is typically prepared with a part of water 24 h prior to mixing and blending with the rest of water just before use.

In recent years, there has been increasing interest in incorporating alkali activators in the solid phase (one-part AABs), offering the potential to market a "dry bag" of alkali-activated cement, similar to commercially available PC [4]. However, in two-part AABs, preparing alkali activator solutions 24 h in advance results in a more homogeneous AAC mix, suggesting that while the one-part method simplifies non-hazardous handling, the two-part method may yield better mixing consistency.

Within the broad group of AABs, there are two main sub-classes: high-calcium systems and low-calcium systems. For the development of new standards to be applied for different alkali-activated systems (i.e., low-calcium, high-calcium and blended), the type of precursor material must be considered when establishing new correlations [48]. In GGBFS-based AAB, the main hydration product is a calcium aluminosilicate hydrate (C–A–S–H) gel, which is a typical high-calcium system. Notably, this gel has a lower Ca/Si ratio than hydration products of traditional PC (calcium silicate hydrate: C–S–H). In contrast, the main hydration product of low-calcium binders is sodium aluminosilicate hydrate (N–A–S–H) gel, which possesses a three-dimensional structure [43]. Recent research shows that the higher the pH of the medium, the more C–A–S–H will prevail over N–A–S–H. Likewise, the lower the concentration of alkalis and the more calcium-rich environment, the more C–A–S–H gel will be formed. The morphology of C–A–S–H gel chains in AABs consists of combined reticular network and honeycomb structure similar to the C–S–H gel in PC. However, the difference lies in the inclusion of aluminium in their structure of C–A–S–H gel, which replaces some of the silicon in the bridging positions [4]. More detailed information for this research topic can be found in Chapters "Conventional Precursors and Activators" and "Non-conventional Precursors and Activators" [5, 6].

The performance of AABs depends on several factors, such as the type and dosage of the activator, the type and dosage of the precursor, the mixing procedure (which

includes mixing steps and duration), climatic regions, and the curing conditions. Notably, the reactivity of the aluminosilicate precursors in an alkaline environment cannot be solely predicted based on their chemical composition (see Fig. 2, [49]). Various variables must be taken into account to assess accurately and optimize the performance of AABs.

The low-calcium FA appears to be more suitable for AAMs production than high-calcium FA. The primary challenge with high-calcium FA is that they have an extremely fast setting, commonly referred to as flash setting. In contrast, low-calcium FA exhibits low reactivity, necessitating either a higher molarity activator or curing at elevated temperatures, typically between 40 and 80 °C. Recent studies have indicated a preference to elevated temperatures, as it helps to mitigate the rapid setting issue. Usage of lower molarity activators allows for better control over the setting process.

As coal-power plants transition to renewable sources such as wind, solar or biomass in the forthcoming years, the generation of coal FA is expected to decrease significantly by 2035. However, the situation varies by country and government policy. For example, the UK closed the last coal power station in September 2024—as the first G7 country to phase out the coal power. As of 2024, the member countries of the G7 (Group of Seven) are: USA, Canada, Germany, France, the UK, Italy and Japan. Germany and Japan, for example, have been granted more time to fully transition away from coal, reflecting their current dependence on this energy source. Likewise, world's largest coal producers and consumers—Australia (26%), China

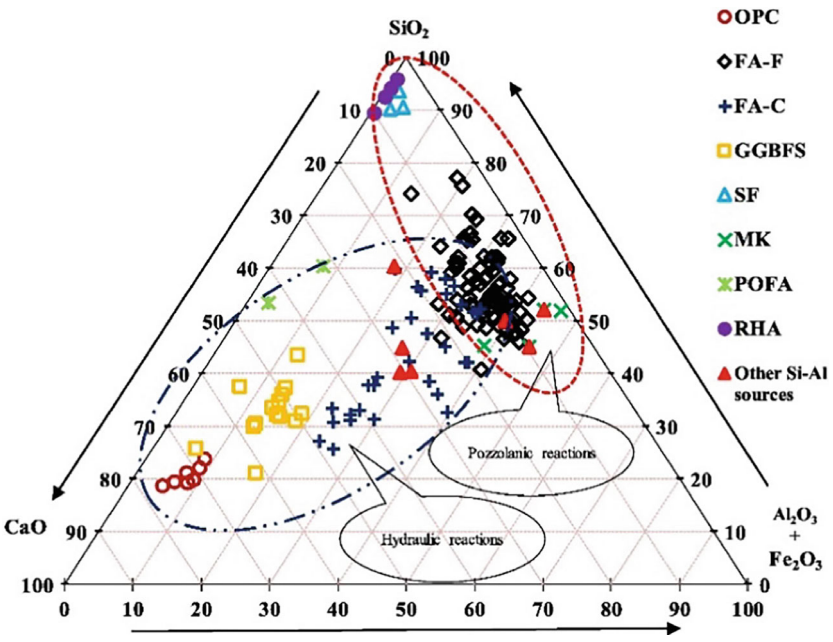

Fig. 2 Ternary diagram of source materials for traditional PCC and AAC [49]

Table 2 Summary of satisfactory combinations of solid precursors and alkali activators [3]

Precursor	MOH	$M_2O{\cdot}nSiO_2$	M_2CO_3	M_2SO_4
GGBFS	Acceptable	Desirable	Good	Acceptable
FA (low Ca content)	Desirable	Desirable	With clinker	With clinker
Calcined clays	Acceptable	Desirable	With clinker	With clinker
Natural pozzolans	Acceptable	Desirable	–	–
Steel/phosphorus slag	–	Desirable	–	–
Copper slag	–	Acceptable	–	–
Red mud	–	Acceptable	–	–
Incinerated solid waste	–	Acceptable	–	–

(55%), India (55%), Indonesia (45%), Russia (11%), South Africa (69%) and USA (10%)—continue to rely on coal for their energy needs. Using the stockpiled FA as an aluminosilicate source for AAMs production addresses the environmental problem of landfills by reducing them. However, the main drawback of using stockpiled FA is that it might contain impurities and moisture, necessitating extra pre-conditioning procedures [16]. For this reason, many cement manufacturers prefer FA sourced directly from the power stations to minimize handling costs [4].

Extensive research from the literature regarding adequate combinations of precursors with alkali activators was presented by Provis et al. [3] and is summarized in Table 2.

2.4 Environmental Sustainability of AABs

LCA is a method utilized to assess the environmental aspects and potential consequences of a product, aiding in rational decision-making [50]. AABs have gained attention for their environmental sustainability, which can be effectively demonstrated through LCA [51]. Precursors and activators play a significant role in determining the environmental impact of AABs. Industrial residues are commonly used as precursors, while sodium silicate (SS) and sodium hydroxide (SH) serve as alkali activators. These two commonly used alkali activators constitute 1–5 wt.% (SH) and 3–10 wt.% (SS) in one m^3 of AAC [4]. Alkali activators are the main contributors to the total global warming potential (GWP) of AAMs mixes, accounting for nearly 60% of CO_2 eq. emissions [52].

LCA studies can be difficult to compare due to variations in methodologies, functional units and scope of each study. A comprehensive assessment that includes different combinations of precursors and activators is essential for partial evaluation of the environmental sustainability of AABs. Table 3 presents a literature review summarizing the findings from LCA studies conducted on AABs. Various combinations of precursors and activators have been studied, showing reductions in

GWP, emissions of greenhouse gases (GHGs), and energy consumption compared to PC. However, the environmental benefits of AABs are not consistently superior in all impact categories when compared to PC, and the choice of activators greatly influences the environmental impact.

At the same time, there remains ongoing debate about the best practices conducting fair and representative LCA analyses for AAC. The recyclability of AAC is still not well understood, complicating its incorporation into LCA studies. Conversely, different studies may use varying definitions of the functional unit, often opting for m^3 AAC, which may not adequately reflect structural performance differences between AAC and PCC.

2.5 Alkali-Activated Concrete

Several challenges and limitations associated with the use of AAC are reflected in Sect. 2.2 of this Chapter. Like PCC, AAC hardens and develops its mechanical properties over time from a fresh state. At the mesoscale, they both contain a binder, aggregates, and aggregate-binder interface. On structural macroscale, both may be either reinforced or prestressed. As noted earlier, PCC codes may not fully address AAC properties, therefore more attention should be focused on the incompatibility between traditional codes and distinctive characteristics of AAC. When considering the mechanical behaviour of AAC, the same test procedures used for PCC are applied by default to AAC testing strengths (compressive [69, 70], splitting tensile [71, 72], flexural), stiffness, i.e., Young's modulus and Poisson's ratio [73, 74]. However, AACs exhibit distinct volume stability, making it crucial to consider loading rates to eliminate creep effects. The linearity of stress–strain behaviour is debated, raising questions about using EN and ASTM standards for determining elastic modulus and testing creep. AAC's higher shrinkage increases the impact of eigen stresses, which are influenced by specimen size and boundary conditions. GGBFS-based AAC is more prone to size-dependent carbonation and drying shrinkage, making specimen size more critical than in PCC testing.

2.6 Production Methods of AAC

As was mentioned before, the conventional approach has involved blending alkali activators with the precursor in the liquid phase, thus employing a two-part mixing method. However, contemporary attention has been redirected towards incorporating alkali activators in the solid phase, known as a one-part mixing method, promoting subsequent dissolution by pre-grinding them together with the precursor to decrease their particle size.

In both production methods, the pre-treatment of industrial by-products such as FA and GGBFS typically involves drying and grinding steps to homogenize the

Table 3 The findings from LCA studies conducted at AAB

References	Mix type	Precursors	Activators	Reference PC	Impact categories	Basis for inventory data	Allocation	System boundaries	Concrete, functional unit	Findings
[53]	Two-part AAC: GGBFS/FA ratio 80:20	FA, GGBFS	SS + SH	Freeze-thaw resistant concrete according to [54, 55]	3 indicators: ADP, GWP, CED	Ecoinvent, literature, industry	No allocation	CtG	1 m^3	Improvement on GWP, but similar impact on ADP and CED
[56]	Two-part AAC: FA (8 ref, 48 mixes), GGBFS (4 ref, 12 mixes), MK (4 ref, 17 mixes)	FA, GGBFS, MK	SS + SH	Equivalent compressive strength	10 indicators	Ecoinvent, literature, industry	No, mass, economic	CtG	1 m^3	Higher impacts in other category than global warming
[57]	Two-part AAC	FA + silica fume (SF)	SS + SH	100% PCC (2); PCC and GGBFS (2); PCC and FA (2)	Energy, greenhouse emissions and cost	Literature, calculation	No allocation	CtG	1 m^3	Results depend on the transport distance
[58]	Two-part mixes GGBFS (3), AA FA (3), AA-MK (1)	FA + GGBFS or FA + MK	$Ca(OH)_2$ + SS or SS + SH	100% PCC (3); PC + supplementary cementitious material (3)	CO_2 footprint	Korea Life cycle inventory database information network, Japanese database	No allocation	CtPCt	1 m^3: 24, 40, 70 MPa	Favourable to AACs
[59]	Two-part GGBFS-based AAC, 7 mixes: 3 PCC and AAC with 20, 30, 35 MPa strength, each GGBFS-based AAC with 35 MPa	GGBFS	SS, SH	Equivalent compressive strength	EIO method, and TRACI	NREL, Ecoinvent, Granta EduPack, literature	Mass and economic allocation	CtG	1 m^3: specific compressive strength	GGBFS-based AAC achieved considerable environmental impact reductions except for ODP and ecotoxicity. This is attributed to the alkali activators

(continued)

Table 3 (continued)

References	Mix type	Precursors	Activators	Reference PC	Impact categories	Basis for inventory data	Allocation	System boundaries	Concrete, functional unit	Findings
[60]	Two-part AAC	Natural pozzolan, GGBFS	SS + SH	Equivalent mix proportions	GWP 100, GTP 100	Ecoinvent	No allocation	CtG	1 m^3	AAC with natural pozzolan and GGBFS exhibited a reduction of 44.7% in GWP compared to PC activating solution contributes to approximately 85% of emissions of AAC
[61]	Two-part AA paste; 6 mixes: 1 PC, 5 AAB with different NS content	Waste brick powder	SS + SH	Equivalent compressive strength	Energy consumption, CO_2 emissions	Literature, industry	No allocation	CtG	1 m^3 paste	AAB mix with optimum mix proportions and strength equivalent to PC resulted in 63% and 81% lower consumed energy and GHG emissions, respectively compared to PCC
[62]	One-part AAS mortar: 2 mixes with 2 different activators	GGBFS	Desulfurization-dust + SS, SH	Equivalent compressive strength	ReCiPe midpoint	Ecoinvent	No allocation	CtG	1 m^3: 30 MPa	Replacing SH with desulfurization-dust as an activator resulted in a considerable reduction (≈99%) for all impact categories

(continued)

Table 3 (continued)

References	Mix type	Precursors	Activators	Reference PC	Impact categories	Basis for inventory data	Allocation	System boundaries	Concrete, functional unit	Findings
[63]	Two-part fiber reinforced AAB; 5 mixes, 3 different fibers	FA, GGBFS	SS + SH	Equivalent compressive strength	CML 2015	Literature, GaBi	No allocation	CtG	$1m^3$	Steel, waste glass and PP fiber reduced the emissions by 16%, 23%, and 0.8%, respectively. Glass fibers are environmentally more sustainable
[51]	Two-part AAC; 7 mixes: 1 100% PC, 2 PC mixes with 33% replacement of GGBFS and NP, 3 AAB mixes with 3 different activators	GGBFS, natural pozzolan	Na_2SO_4, Na_2CO_3, SH	Equivalent mix proportions	GHGs emissions, air pollutants	US government University of California Berkeley Green Concrete tool, LTS database, literature, NREL	No allocation	CtG	1 m^3 mortar	GHGs emissions of AAC depended on mix design and the raw materials. Na_2SO_4 mix resulted in lower GHGs emissions
[64]	Two-part AAC; 4 mixes; 1 PCC, 1 FA-based AAC, 1 AAC: FA + SF, SS + SH; 1 AAC with FA, SF	FA + SF	SS + SH, SH + SF	Equivalent mix proportions (paste volume and paste/ aggregates)	ReCiPe midpoint and endpoint	Ecoinvent	No allocation	CtG	1 m^3	Substitution of SS with SF reduces the environmental impacts, but the difference in endpoint indicators of AAC is not significant. Transportation distances affect AAC more than PCC
[65]	Two-part AAC	FA, GGBFS	SS + SH	Equivalent compressive strength	ReCiPe midpoint and endpoint	Ecoinvent	No allocation	CtG	1 m^3	Transportation and sodium silicate, contribute the most to midpoint damage categories in various mixes of AAC

(continued)

Table 3 (continued)

References	Mix type	Precursors	Activators	Reference PC	Impact categories	Basis for inventory data	Allocation	System boundaries	Concrete, functional unit	Findings
[66]	One and two-part 4 mixes S1—one-part mortar (conventional powder activator) S2—two-part mortar (conventional aqueous activator) S3—one-part mortar (WG-NaOH derived powder activator) S4—two-part mortar (RHA-NaOH derived aqueous activator)	FA, GGBFS	Waste glass (WG) + SH, rice husk ash (RHA) + SH, SS + SH	Midpoint hierarchist timeframe	ReCiPe 2016	Literature, GaBi, Ecoinvent	No, mass allocation	CtG	1 m^3 of AAMr with compressive strengths between 52 and 60 MPa at 28 days	SS is the most significant contributor, while WG and RHA-based alkali-activated mortar showed lower emissions across all impact categories. SH from the technology mix resulted in lower emissions
[67]	Two-part AAC, 100 FA, FA/RHA of 90:10	FA + RHA	SS + SH	Equivalent compressive strength	As per ISO 14044 [68] and GHG emissions	Industry, literature, calculation	No allocation	CtC	1m^3	12% reduction in GHGs emissions with the use of AAB. The primary contributor to environmental impact is an alkali activator

Note CtG—Cradle-to-Gate, CtC—Cradle-to-Construction stage, CtP—Cradle-to-Preconstruction stage, ADP—Abiotic depletion potential, ODP—Ozone depletion potential, CED—Cumulative energy demand, GTP100—Global temperature change potential over 100 years, EIO—Economic Input–Output, TRACI—Tool for Reduction and Assessment of Chemicals and Other Environmental Impacts, NREL—National Renewable Energy Laboratory, AAMr—Alkali-activated mortar, NP—Natural pozzolan, SF—Silica fume, NS—Nano silica, WG—Waste glass, RHA—Rice husk ash

material and increase its reactive surface. Following the alkali activation of these pre-treated precursors, inert aggregates such as sand and gravel are added into the mixer to form AAC. Admixtures are commonly included in PCC to control setting and hardening, and to improve durability. These commonly applied admixtures are superplasticizers, accelerators, or retarders, although their universal application in AAC production is not assured [75]. After homogenously blending of all raw materials, the fresh AAC can be either precast with controlled conditions or cast in-situ at the construction site. Subsequently, AAC undergoes setting, hardening, and strength-gain over time. The curing period is crucial for the long-term properties of AAC in the surrounding environment, therefore protective measures to control moisture loss, maintain temperature, etc. are considered [4].

2.7 AAC Mix Design

AAC mix design is vital for its production. AAC comprises a wide range of mate-rials, with unknown fresh and hardened-state properties, making it challenging to engineer the mix effectively. Unlike PC systems, which have established and standardized mix design approaches like the Paoluomi formula (i.e., indicating that water-to-binder (W/B) ratio dominates concrete compressive strength) or other standard codes [76–79], AAC lacks a universally accepted method for proportioning its mixes. The composition of raw materials and mix proportions (e.g., type and dosage of activators and precursors) significantly influence the final performance of AAC. The existing research on AAC often employs tailored mix designs to each investigation, thereby complicating the replication and comparison. It is now more important than ever to recognize that computer modelling has transformed the field of civil engineering, and it can be effectively applied even within the constraints of real-world laboratory. For instance, the research conducted by Volker et al. [80] applied Sequential Learning optimization to identify optimal AACs, focusing on critical factors such as data limitations, ecological considerations, model comparisons and prediction techniques.

The current production of AAC is mainly based on the so-called “empirical design method”, in which empirical data of the W/B ratio, aggregate content, etc., are used for the decision of initial mix proportions. While most mix design guidelines for PCC are empirically established, making upfront design challenging, the underlying mechanisms and the role of mix design parameters are better defined, leading to a more comprehensive understanding of PCC compared to other materials. Subsequent iterations involve conduction of multiple trial mixes and their adjustment until AAC’s necessary properties are achieved. While this procedure offers simplicity in execution, it demands intensive trial-and-error work to obtain optimal mix proportions. Moreover, any change in source materials or application situation requires intensive re-testing and adjustments. It might be difficult to investigate the influence of all the parameters in a single investigation. However, employing a well-designed experimental series, such as the Taguchi method, has facilitated the thorough examination

of six factors at four levels each, investigating their influence on AAC mix design (see Fig. 3) [81].

The literature indicates that AAC mix design is a complex process due to numerous variables like alkaline content [82], curing time [49] and temperature [83], water-to-solid (w/s) ratio [84], pH and molarity of activators [85], aluminosilicate composition and type [86], aluminates to silicate ratio [87], and silicate to hydroxide ratio [88] involved in the alkali-activation process [84]. Since a universally accepted approach for proportioning AAC mixes is lacking, overlooked factors like the specific gravity of raw materials (the total aggregate content or the fine and coarse aggregate content based solely on weight) lead to inconsistent results when binder and aggregate properties are changed [89]. It is crucial to understand the significance of individual parameters on AAC performance and develop a framework for mix proportioning. Existing literature reports various mix design procedures for AAC, including the target strength method (TSM) with fixed water content [40, 41], fixed binder content [43, 48], fixed paste content [49, 50], multivariate regression models [53, 56], packing fraction of raw materials and paste thickness [90], Taguchi method [18], Taguchi-based TOPSIS method [91], and reactive modulus approach [92].

A mix design approach based on the TSM following the ACI 211.4R-93 approach [93] is employed to formulate alkali-activated high-calcium FA concrete. The mix design procedure involves parametric studies investigating the effects of various factors, including different NaOH concentrations, alkali activator solution to binder ratios, and coarse aggregate size [94]. The mix design process is visually represented in Fig. 4, illustrating the step-by-step flow of the procedure.

Although Rafeet et al. [95] have made efforts to develop a mix procedure to achieve the target strength, setting times, and workability of FA-based AAC, their study did not adequately consider the most critical parameters, such as the type and dosage of activators, as well as the shape and grading of aggregates. Most mix proportioning methods for AAC primarily rely on statistical approaches that empirically predict

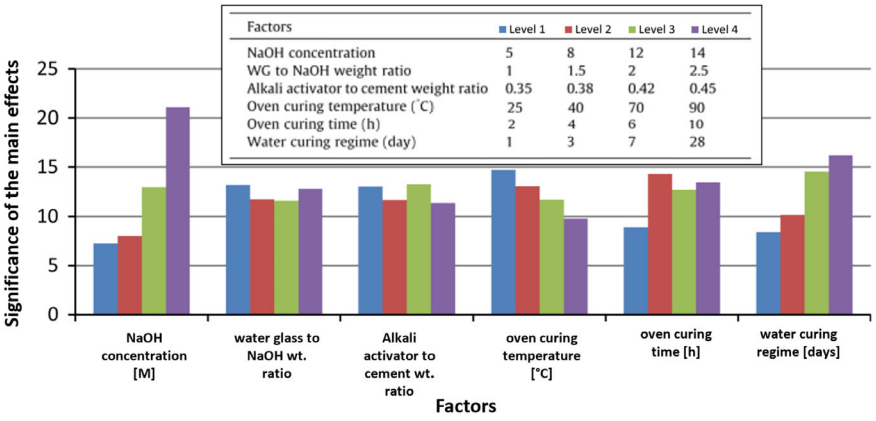

Fig. 3 The significance of the main effects for six factors in four levels [81]

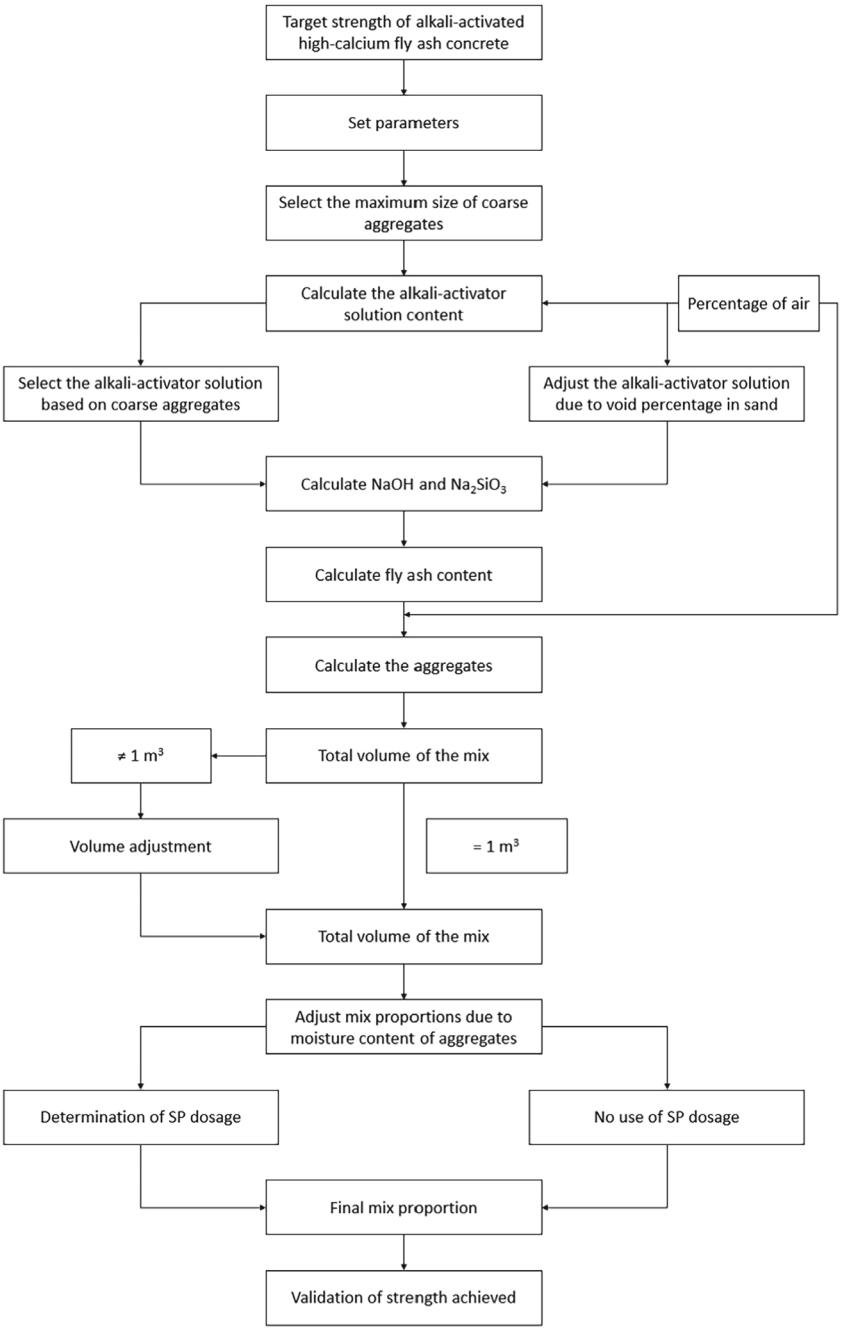

Fig. 4 Mix design flowchart proposed by Phoo-Ngernkham et al. [94]

the properties of AAC based on their mix proportions. However, several limitations have been identified when using these methods to develop AAC mixes. Bondar et al. [90] proposed a particle packing approach specifically aimed at achieving a relatively low activator content for producing structural GGBFS-based AAC, as illustrated in Fig. 5.

The Taguchi method, a widely recognized experimental design approach, has been recommended as a functional tool for considering the effects of multiple parameters [96]. Researchers such as Riahi et al. [97], Olivia et al. [98] and Hadi et al. [99] have applied the Taguchi method to investigate various aspects of FA-based AAC, including the influence of sodium hydroxide concentration, curing conditions, and parameters related to alkali-activator composition and dosage. Additionally, Li et al. [18] proposed a mix design framework, as depicted in Fig. 6, for proportioning AAC mixes.

The findings derived from widely accepted and reported investigations of FA-based AAC highlight several key observations [100–103]. Firstly, the w/s ratio has an inverse relationship with the strength of AAC. Secondly, the alkaline liquid/binder ratio directly affects the workability of AAC. Thirdly, the strength of AAC varies with curing duration and temperature range depending on the precursor used in the production. Fourthly, dry curing methods which include sealing of specimens tend to yield

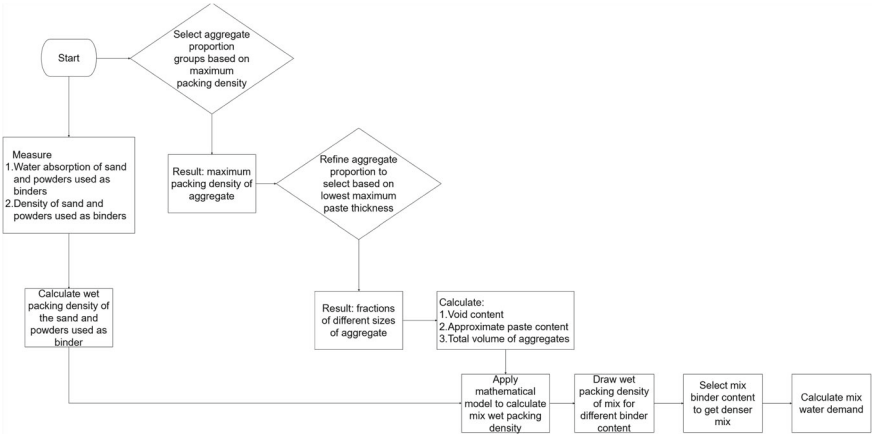

Fig. 5 Mix design procedure for GGBFS-based AAC proposed by Bondar et al. [90]

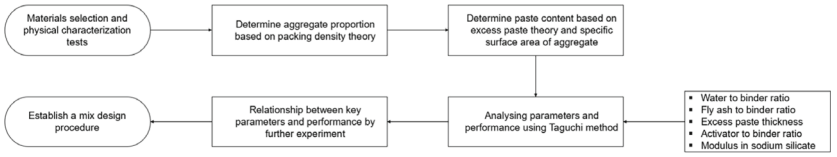

Fig. 6 Flow chart for the proposed principles for composition design of FA-based AAC proposed by Li et al. [18]

higher strengths compared to wet curing methods at similar temperatures. Furthermore, higher silicate-to-hydroxide ratios contribute to increased strength, albeit at the expense of higher unit costs for the AAC system. Lastly, it is recommended that the ratio of SiO_2/Na_2O in the sodium silicate solutions should be around 2.0. Junaid et al. [104] have highlighted the interdependence of the w/s ratio and alkaline liquid/binder ratio in the engineering of AAC mixes with satisfactory strength and workability. They have introduced G-graphs as a tool to facilitate the design of FA-based AAC mixes (Fig. 7). These graphs provide an overview of the proposed mix design approach and aid in achieving desired performance outcomes for AAC.

Xie and Zhao [92] have introduced a mix design methodology that employs the reactive index concept. The reactive index is composed of the five major oxides found in the reactive ingredients in AAC (namely CaO, Na_2O, SiO_2, Al_2O_3, and Fe_2O_3) and other critical mixing parameters, such as w/s ratio, paste-to-aggregate volume ratio, and coarse-to-fine aggregate volume ratio. Their approach uses a unified model to forecast the compressive strength of AAC at different temperature intervals.

A step-by-step method for AAC mix proportioning by Li et al. [18] is shown in Fig. 8. Properties considered are slump, setting times and compressive strength.

The existing mix design procedures struggle to accommodate variations in the physical characteristics of binder and aggregate materials. In PCC, compressive strength is determined by paste, aggregates, and interfacial transition zone (ITZ)

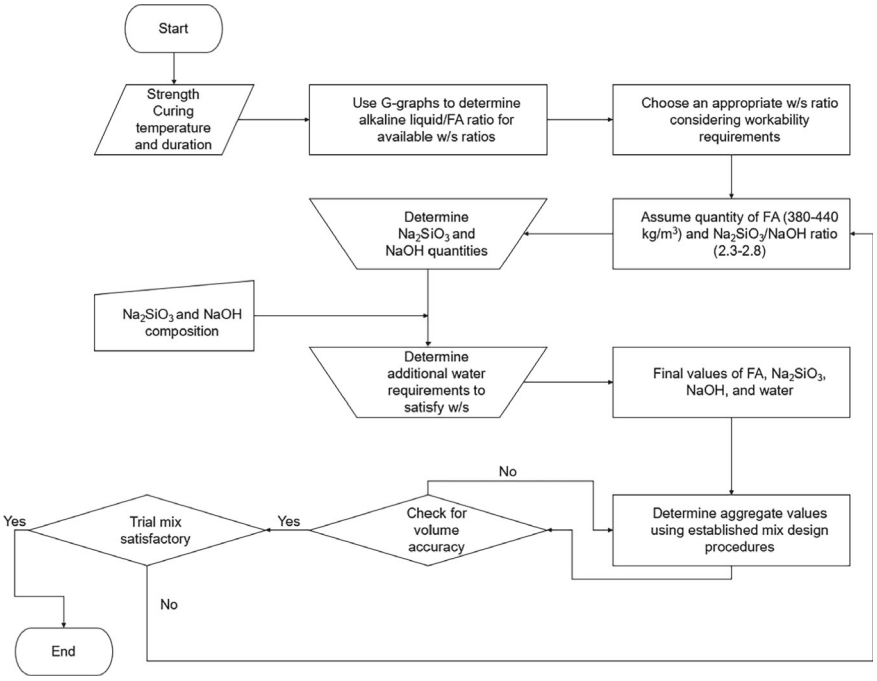

Fig. 7 Proposed mix design approach by Junaid et al. [104]

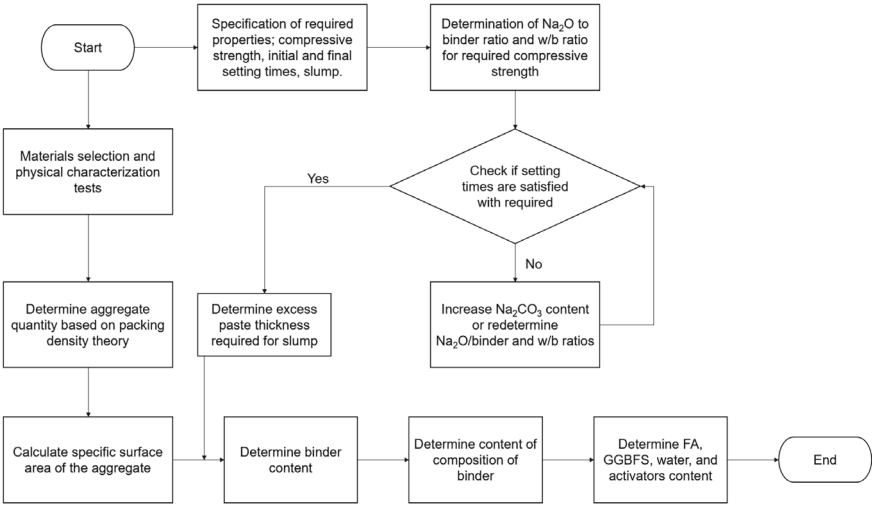

Fig. 8 Flow chart for the application of the mix proportioning method by Li et al. [18]

porosities. However, standards like ACI 211.1-91 [79] and EN 206 [54] primarily focus on paste porosity assuming aggregate porosity is low, and the transition zone's effect is negligible, even though it could be the weakest link. In GGBFS/FA-based AAC, the aggregate is often stronger than the paste, and the interfacial transition zone is denser and more cohesive than in PCC. This is due to higher bonding from soluble Si in the alkali activator and the formation of reaction products with lower Ca/Si ratio, reducing cracks in the transition zone [105].

Fixed weight-based approaches or empirical models results in unreliable and irreproducible AAC production outcomes. To overcome these limitations, there is an urgent need for a more comprehensive and robust mix design procedure for AAC. This procedure should incorporate systematic consideration of all pertinent parameters, including activator type and dosage, aggregate characteristics, and alkaline liquid/binder ratio. Statistical methods, such as the Taguchi method, can effectively explore and evaluate the effects of multiple parameters. Implementing such a procedure can ensure the cost-effectiveness, workability, and required mechanical properties of AAC, making it a viable alternative to PCC. Like, for example, in the study by Sun et al. [105] (see Fig. 9).

2.8 Workability

For GGBFS-based AAC, the design and control of setting time are particularly important. A rapid loss in workability (usually setting in less than 30 min) was reported for GGBFS-based AAC, which is a notable limitation in its field applications like

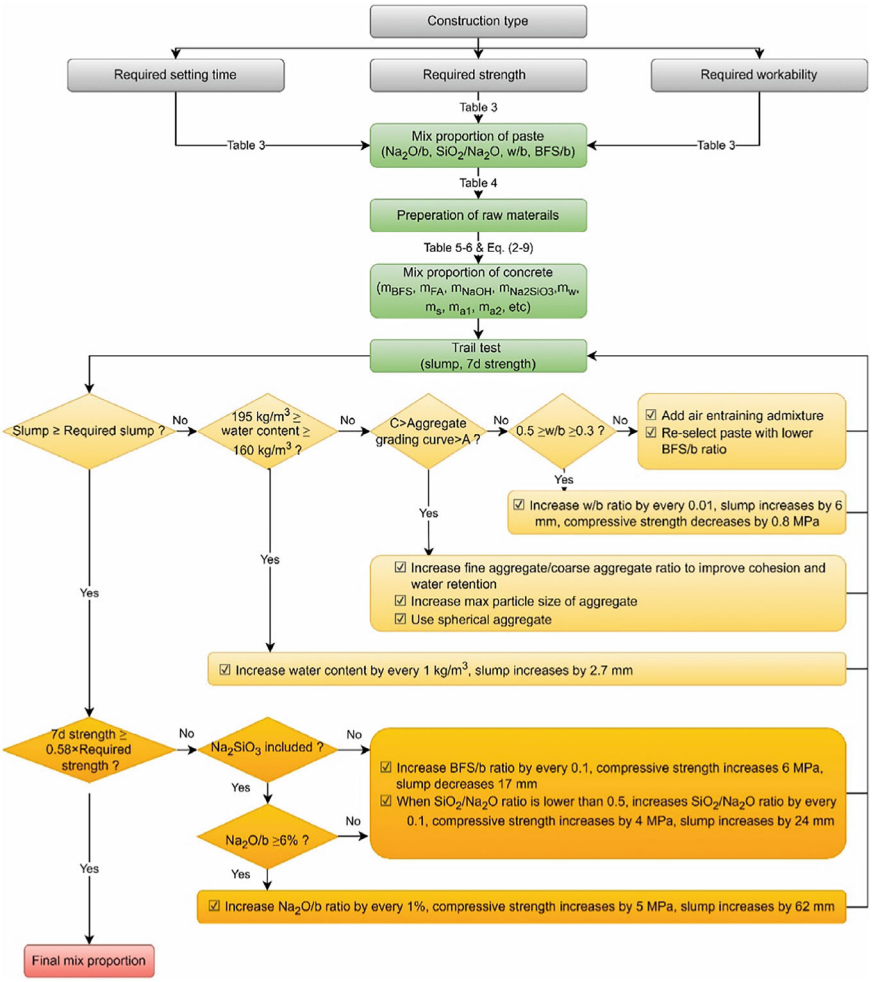

Fig. 9 Mix design procedure of GGBFS/FA-based AAC [105]

ready-mix and pumped concretes [106, 107]. Flash setting occurs in AAC because of either the heat generated from the dissolution of solids in the alkaline solutions, or the high calcium content of the source materials [49]. Various methods have been attempted to avoid the flash setting of binders in AAC, with the majority adopting the approach of adjusting the mix proportions of AAC or the binder constituents to attain more desirable rheology.

The approaches to adjust mix proportions include reducing calcium content in the binder, adding extra water, varying total w/s ratio, SS to SH ratio, SH concentration or silica modulus of SS solution (e.g., SiO_2/Na_2O weight ratio). While changes in mixing proportions have been found to delay setting, mechanical properties of AAC might also be compromised. It must be noted that the commonly applied admixtures

for PCC might not be compatible with AAC [3]. For instance, a lignosulfonate admixture improves workability but may cause retarded strength development and reduced flexural strength of GGBFS-based AAC [108]. Therefore, it might be worth considering the method of adding admixtures and alkali activators separately [109]. It is worth noting that in most cases, the conventional retarders applied in AAC mixes are similar to those commonly used in conventional PCC, such as natural sugar/glucose, phosphoric acid (H_3PO_4), gypsum ($CaSO_4 \cdot H_2O$) and citric acid ($C_6H_8O_7$). However, due to the differences in reaction mechanism and kinetics between the AAC and PCC binders, these conventional retarders only affect the setting of high calcium-containing AABs in AAC, while being less effective at delaying setting of those with low calcium content. This is simply because these conventional retarders only prolong the time to form hydrates associated with the reactions involving calcium ions.

The setting time can be controlled by adjusting the GGBFS content through careful composition design or by introducing CaO in proper forms within alkali-activated SiO_2–Al_2O_3–CaO solid precursor system [110]. The workability of GGBFS activated by Na_2CO_3 was found to be greater than that activated by sodium silicate [111]. Both the Na_2O/binder (N/B) ratio and W/B ratio are the key parameters affecting the setting times of GGBFS-based AAC. To better control the setting time, sodium carbonate can be used to partially replace sodium silicate. In a study by Li et al. [18], the setting times of GGBFS-based AAC was prolonged to 1–2 h with the replacement of sodium silicate by sodium carbonate at a 2% Na_2O_{eq} content. However, it is essential to consider the impact on slow strength development as well.

More detailed information for this research topic can be found in Chapter "Fresh AAM Properties" [75].

2.9 Curing Conditions

GGBFS-based AACs gain high strength when cured at ambient temperature whilst requiring relatively low activator dosage [38, 112], unlike FA-based AACs, which in some cases have been observed to require high alkali dosage (6–10% Na_2O_{eq} content) and/or elevated curing temperatures (40–100 °C) to achieve suitable mechanical properties [104, 113].

Singh et al. [114] studied the effect of heat curing (80 °C) and ambient curing (27 °C) on a mix of a FA/GGBFS aluminosilicates regarding the strength development. Initially, the heat cured specimens (80 °C) showed higher compressive strength after 7 days due to the heat release during both the alkali-activation and heat curing process. However, by 28 days, the specimens cured at 27 °C temperature exhibited higher compressive strength than those cured at 80 °C due to the formation of C–S–H or C–A–S–H. The authors [114] attributed this behaviour to the inhomogeneity of microstructure and the increase of cumulative pore volume of AAC at heat-curing. The microstructure analysis revealed that heat-cured specimens had rough microstructures with voids distributed throughout the surface, while the

ambient-cured specimens exhibited smooth, compact, and microstructure with low void content possibly explaining their superior strength at 28 days.

Bakharev et al. [115] similarly observed that heat-cured AAC specimens developed early strength (i.e., first day strength) more rapidly than specimens cured at room temperature. However, the later strength of heat-cured specimens was slightly reduced, which was correlated with the inhomogeneity in the microstructure of the gel. This was because the rate of reaction exceeded the rate of diffusion, causing most of the hydration products to remain near the GGBFS grains, and leaving interstitial space relatively open, and denser precipitates might potentially form a barrier for ion diffusion, resulting in microstructural inhomogeneity. Additionally, heat curing of GGBFS-based AAB mortar specimens led to a reduction in the compressive strength compared to the ambient curing [47].

Aliabdo et al. [116] cautioned against heat curing for GGBFS-based AAC due to its impact on the formation of C–S–H, which is influenced by temperature. The increase in dry curing temperature leads to more water evaporation, affecting C–S–H formation unfavourably. Likewise, Memon et al. [117] found that while increasing the curing temperature from 60 to 70 °C, the compressive strength of GGBFS-based AAC increased, but temperatures beyond 70 °C led to a decrease in strength. For FA-based AAC, curing temperature accelerates polymerization and significantly affects mechanical strength. Collins and Sanjayan [35] reported that AAC specimens subjected to bath curing continued to gain compressive strength even up to 400 days, whereas the sealed AAC specimens showed minimal strength improvement after 91 days. In contrast, AAC subjected to ambient air exposure curing may exhibit strength retrogression due to the formation of micro-cracks in the matrix. Chi [118] reported that AAC cured at the relative humidity of 80% RH and temperature of 60 °C exhibited the highest compressive strength at the age of 28 days, followed by AAC cured in air and then by AAC cured in saturated limewater.

Jittin et al. [47] reported that specimens cured in lime water achieved compressive strength of 68.2 MPa. This could be attributed to the proper hydration of GGBFS and full pozzolanic reaction under lime water curing conditions. In addition, high humidity curing conditions were reported to be more beneficial than dry conditions, since moisture retention is required for hydration [119]. This finding appears controversial to earlier statements mentioned above [100–103]. The lowest strength was observed for AAC specimens cured under ambient conditions. Specimens cured at 25 °C exhibited higher strength compared to the AAC specimens cured under natural conditions.

3 AAC Mechanical Properties

The performance of the binder in AAC is influenced by several factors, including the choice and combination of precursors (in terms of type, reactivity, and quality) and activators, along with curing conditions. The result of this is an intrinsic variability in the material properties among different types of AAC and in comparison, to PCC.

This section provides an overview of the development of mechanical properties (such as compressive, splitting tensile and flexural strengths) and elastic properties (such as Young's modulus and Poisson's ratio) of AAC. The focus is on the type of curing and the development of these properties over time. The study is limited to binders based on FA, GGBFS or a combination of both. A summary of selected relevant studies is given in Table 4, outlining the effects of activator type, GGBFS to FA proportions, and curing regimes on the development of the material properties of AAC in comparison to PCC control specimens or estimates from PCC-based codes. A detailed comparison of hardened properties is also provided for further discussion.

3.1 Compressive Strength

Compressive strength is a fundamental mechanical property of concrete, which allows its characterization and classification, facilitating the comparison of performance between different concrete types. Compressive strength of AAC originates from the effective density, space-filling, and binding capacities of the precipitating phases such as C–A–S–H gel and Mg–Al layered double hydroxides. The porosity and microstructure of the hardened binder are correlated with its compressive strength, while the reactivity degree of the solid raw material significantly impacting AAC's mechanical performance. Despite the possibility of developing several mix design formulations using the same binder types and alkaline solutions, defining a generalized trend for AACs remains challenging.

It was reported by Sofi et al. [131] that the 28-day average AAC compressive strength closely approached the design strength of PCC of similar density. The similar stress–strain relation in compression to PCC was achieved with the same aggregate type by Nath et al. [125]. Yang et al. [129] reported also a similar rate of strength increase to PCC and compared the stress–strain relationships in compression of GGBFS-based AAC (with W/B < 30%) with predictions by the *fib* Model Code 2010 and the modified Hognestad's model (see Fig. 10) [129]. The stress–strain relationship defined in EN 1992-1-1 [128] has more brittle post-peak behaviour. The behaviour of the AAC mix aligns well with the modified Hognestad's model, whereas it displays lower stiffness and a slower drop of strength in the descending branch as compared to the *fib* Model Code 2010 model [124]. This must be approached also with caution as the testing methods, strain control during the post-peak phase, and boundary conditions significantly impact the results. In general, the initial stiffness of AAC increases with compressive strength, like for PCC.

Some GGBFS/FA-based AAC specimens cured under ambient conditions continued to develop strength after 28 days [125]. The assessment of alkali-carbonate GGBFS-based AAC cylindrical specimens cored from the outer panels of a storehouse in Krakow (Poland), after 25 years suggested a significant increase in compressive strength over time compared to 28-days [3]. On the other hand, a 17% decrease in compressive strength is reported between 56 days and 1 year for GGBFS-based AAC specimens exposed to 50% RH and 23 °C after demolding [35]. Wardhono

Table 4 Overview of the studies focused on the mechanical properties of AAC

References	Precursor		Activator			Control sample	Description of study
	GGBFS (%)	FA (%)	NaOH	Na_2SiO_3	Other		
[120]	100% high MgO GGBFS	0	–	√	Na_2CO_3 10% weight	–	Compressive strength at 3, 7, 28, 180 and 360 days. Drying shrinkage of unsealed specimens after final setting (1 day for heat curing, 2–3 days lab conditions) and creep tests of sealed specimens for 28 days. Specimens tested at 20 °C ± 2 °C and 40% ± 7% RH
[121]	100 50	0 50	–	√	–	CEM I 52.5N CEM III/A 42.5LA CEM III/B 42.5HSR LA	Elastic modulus, compressive and tensile splitting strengths at 1, 3, 7, 28 days. Measurement of autogenous shrinkage and restrained autogenous shrinkage
[122]	50	50	√	√	–	CEM I 52.5R	Measurement of setting time, autogenous shrinkage (7 days), shrinkage under saturated conditions, chemical shrinkage and internal RH and characterization of the microstructure. Monitoring of elastic modulus from casting to 7 days

(continued)

Table 4 (continued)

References	Precursor		Activator			Control sample	Description of study
	GGBFS (%)	FA (%)	NaOH	Na_2SiO_3	Other		
[37]	100 50	0 50	√	√	–	–	Development of material properties (compressive, tensile splitting and tensile flexural strength and elastic modulus) over time (up to around 2 years) and the response to 4-point load tests of reinforced beams with 0.61% reinforcement ratio
[41]	100 50	0 50	√	√	–	CEM I 42.5 N CEM I 52.5 R	The compressive strength, splitting tensile strength, elastic compressive modulus of PCCs and AACs (exposed to drying conditions) are investigated for a duration of 3.5 and 5 years
[123]	100	0	√	√	–	CEM I 32.5R concrete	Autogenous shrinkage at 65% RH of sealed GGBFS-based AAC and PCC, compressive creep of sealed and unsealed specimens. Comparison to *fib* Model Code 2020 [124]
[125]	0	100	√	√	–	2 PCC mixes (ACI 211.1-91)	11 concrete mixes. Additives (GGBFS, PC and calcium hydroxide in small varying proportions) are used to improve the setting properties. Compressive strength, flexural strength and elastic modulus at 28 and 90 days

(continued)

Table 4 (continued)

References	Precursor		Activator			Control sample	Description of study
	GGBFS (%)	FA (%)	NaOH	Na_2SiO_3	Other		
[126]	100	0	√	–	–	Type I Portland cement	Shrinkage of GGBFS-based AAC exposed to four different RH (70, 50, 30 and 11%) and 23 ± 0.5 °C for up to 70 days. Also, characterization of the microstructure is studied
[127]	14.8	85.2	√	√	–	–	Creep and shrinkage of AAC for curing conditions at elevated temperature (40 or 80 °C) and compared to EN1992-1-1 [128] predictions. Compressive strength and elastic modulus were also tested at 28 days
[129]	100	0	–	√	$Ca(OH)_2$ Na_2CO_3		12 mixes. Evaluation of the effect of W/B ratio (25 to 60%) in the 28-day mechanical properties (compressive strength, stress–strain relation, elastic modulus, direct tensile strength, modulus of rupture, shear stress–strain relation, bond stress-slip diagram)
[130]	100–0	0–100	√	√	–	–	12 mixes with a design characteristic compressive strength of 40 MPa at 28 days. Specimens were demolded after 24 h, cured at ambient conditions and tested at 28 days

(continued)

Table 4 (continued)

References	Precursor		Activator			Control sample	Description of study
	GGBFS (%)	FA (%)	NaOH	Na_2SiO_3	Other		
[131]	Varying	Principal	√	√	Na_2CO_3	–	Six mixes. Influence on the mechanical properties when including coarse aggregate and GGBFS. Specimens cured at 30–35°C and 80% RH, demolded after 24 h and then cured at 23°C until testing for elastic modulus, compressive, tensile splitting, and flexural strength at 28 days
[132]	100 70 50 0	0 30 50 100	√ 2 M 10 M	–	–	–	Influence of activator concentration, curing temperature and GGBFS to FA proportion in the strength and hydration products of AAB mortar. Compressive strength at 1, 7, 28 and 90 days, curing at 25 or 65 °C for 5 h and then exposed to ambient temperature and 98% RH

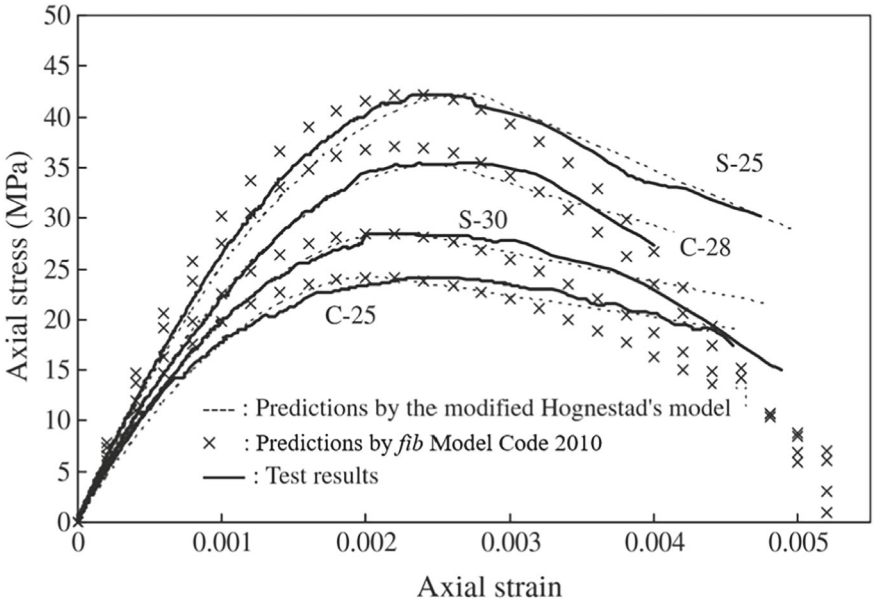

Fig. 10 Stress–strain response of GGBFS-based AAC activated with $Ca(OH)_2$ and W/B < 30% as reported by Yang et al. [129]

et al. [39] observed a slight reduction in strength for GGBFS/FA-based AAC that was water-cured at 23 °C for 6 days and then stored at room temperature until testing. At 180 days, the compressive strength reached 40.2 MPa, with strength remaining above 40 MPa throughout the rest period of the 540 day period. Prinsse et al. [37] exposed specimens to 50% RH after 28 days and investigated the long-term compressive strength. A slight decrease of 5% compared to the 28 day compressive strength was observed for GGBFS-based AAC at the age of 2 years. Additionally, a clear decrease, most pronounced within the first two to five months after being exposed, was observed for elastic modulus (of 20%) and flexural (of 13%) strength over the same lifespan. It was observed that some AACs might be more sensitive to the curing conditions compared to conventional PCC. A study extended to 5 years by Bezemer et al. [41] showed a 22% decrease in compressive strength for GGBFS-based AAC from 2 to 5 years, while control PCC gained strength. Furthermore, while AAC can achieve a similar 28 day strength as per generalized design criteria for PCC structures, this may not always accurately predict its performance over the service lifetime of AAC structure.

The compressive strength of FA-based AAC is directly influenced by the source material and its particle size distribution [133]. Islam et al. [134] studied the compressive strength of GGBFS- and FA-based AACs and found that the maximum compressive strength reached is approximately 66 MPa with the binder composition of 70% GGBFS and 30% FA, respectively. Ranjbar et al. [135] determined that while increasing the dosage of PFA/FA lead to a higher SiO_2/Al_2O_3 ratio, resulting in

reduced compressive strength due to the delayed alkali-activation process. This can be attributed to the early-stage reaction of alumina, leading to a scarcity of Al_2O_3 in the later reaction stages. Iswarya et al. [114] studied the effect of FA/GGBFS ratio on the compressive strength of alkali-activated pastes and found that the strength was higher at a FA/GGBFS ratio of 2:1 compared to 3:1 and 4:1. This increase was due to the denser microstructure. Compressive strength of FA-based AAC increased with the increasing molarity due to the improved polycondensation process [106]. Vora et al. [136] further considered the effect of curing temperature, Na_2SiO_3/NaOH ratio, and alkaline liquid/FA ratio on AAC compressive strength. Increasing the curing temperature resulted in an enhancement of the 7-day compressive strength, while conversely, a rise in Na_2SiO_3/NaOH ratio led to a decrease in compressive strength.

Aliabdo et al. [116] investigated the factors that affect the mechanical properties of GGBFS-based AAC and found that an increase of NaOH molarity led to higher compressive strength due to a rise in alkalinity, resulting in the formation of a higher amount of hydration products. Elyamany et al. [137] evaluated the 7 day strength and setting time of AAC comprising various binders. The authors observed ascending trends in the compressive strength and a decrease in workability of FA-based AAC as molarity increased from 10 to 16 M. Higher Na_2O_{eq} content in the binder generally leads to an improvement in compressive strength [118]. This high Na_2O_{eq} content suggests high alkalinity after mixing with water, contributing to the dissolution of aluminosilicate components and the formation of strength-giving reaction products. Another important factor is activator concentration, followed by curing temperature, and the fineness of the solid raw materials [138].

GGBFS-based AAC can show relatively high early-age strength and rapid strength development due to the quick dissolution of GGBFS particles in alkaline conditions, leading to the rapid precipitation of reaction products. The high mechanical strength of GGBFS-based AAC is attributed to two factors: the matrix and the fast rate of hydration reactions at elevated pH levels, resulting in high early age strength, and a dense and homogenous ITZ with minimal strength differences between the ITZ [139].

The difference in compressive strength between ambient-cured specimens is more pronounced with potassium-based activators compared to sodium-based activators at the same molarity and curing duration [47]. Al-Otaibi [140], Mithun and Narasimhan [141], Bilek et al. [142] and Li et al. [18] obtained AACs with an ultimate strength at 28 days of approximately 80 MPa using a sodium silicate activator. When comparing the experimental results reported by Collins and Sanjayan [38] and Bakharev [115], it seems that sodium silicate solution led to higher early strength than solid sodium silicate powder as an activator.

The N/B ratio is the key parameter affecting the compressive strength of GGBFS-based AAC (Fig. 11). The compressive strength of AAC can reach up to 60 MPa with N/B ratio of 6% (see Fig. 11b, [18]). In addition, the W/B ratio also has considerable influence on compressive strength. Therefore, for strength design purposes, both these parameters must be carefully considered and controlled.

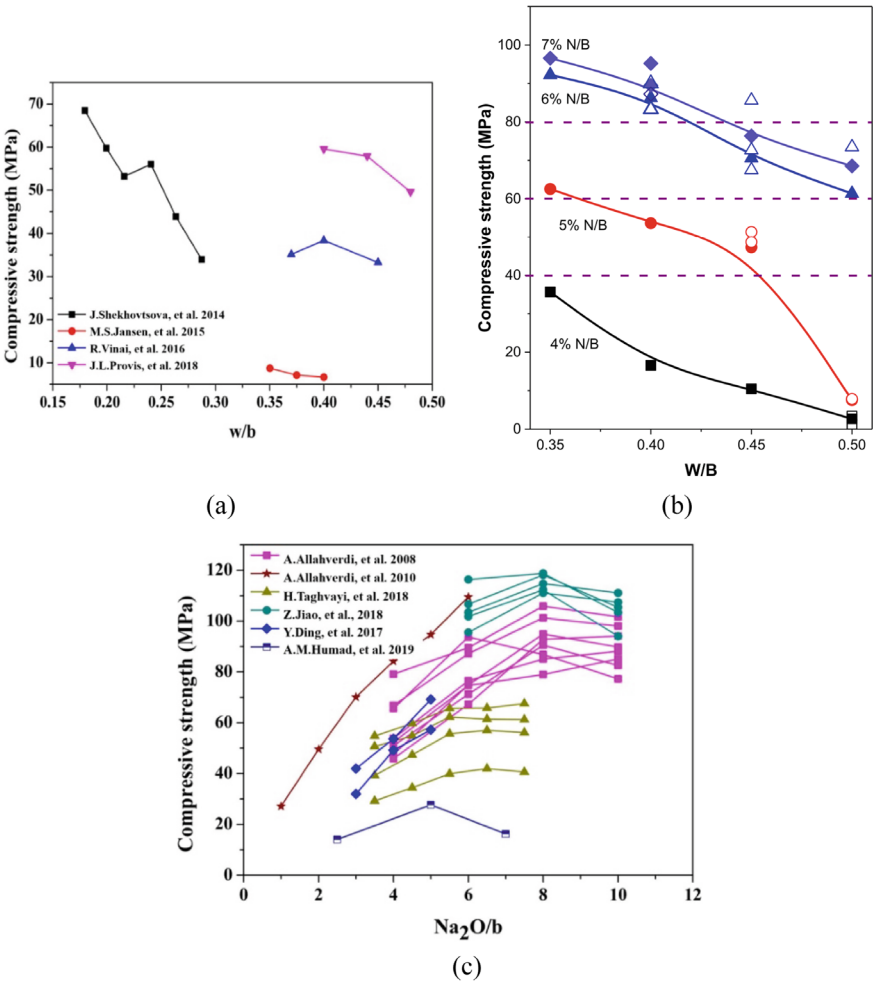

Fig. 11 Compressive strength versus W/B & N/B [18, 143]

3.2 Splitting Tensile and Flexural Strengths

Tensile strength is determined by direct tensile, splitting tensile [71, 72], and flexural tensile tests [144, 145]. AAC exhibits a brittle nature like PCC. Several research studies have yielded conflicting results regarding the splitting tensile strength of AAC due to uncertainties, among other factors, in precursor type and composition, alkali activator type and dosage, curing regimes [112, 129, 146]. According to Deb et al. [147], AAC splitting tensile strength has a direct correlation with its compressive strength. Hence, the effect of different variables on splitting tensile strength was the same as in the case of compressive strength. Ramujee and PothaRaju [148] reported

that the splitting tensile strength of heat-cured AAC is similar to the corresponding strength of PCC, and its relationship to compressive strength is also comparable.

The minimal content of calcium oxide that enables the C–S–H and C–A–S–H formation in the alkali activation process leads to lower splitting tensile and flexural strengths [134]. However, a higher amount of calcium oxide in the precursor facilitates flash setting in AAC.

A few studies have demonstrated the superior splitting tensile strength performance of AAC compared to PCC [149, 150]. For instance, a study conducted by Thomas and Peethamparan [42] demonstrated a splitting tensile strength of 17.0 ± 2.1% of the corresponding compressive strength for GGBFS-based AAC activated with a combination of sodium hydroxide and sodium silicate. These results were significantly higher than those observed for PCC mixes, which exhibited a splitting tensile strength of 14.1 ± 0.6% within a similar strength range. The enhanced splitting tensile strength is attributed to the higher reactivity of GGBFS in the alkaline environment [151]. Chi et al. [118] reported that increasing the dosage of Na_2O positively influenced splitting tensile strength development in all AAC mixes, and the addition of phosphoric acid (H_3PO_4) also enhanced the splitting tensile strength.

Increasing the curing temperature can also enhance the splitting tensile strength of AAC. However, when evaluated without considering the temperature variable, an increase in splitting tensile strength is observed with an increase in the molarity of NaOH [146].

FA-based AAC, cured at 80 °C for 24 h, exhibited 16% greater splitting tensile strength compared to PCC. In contrast, GGBFS-based AAC, using only GGBFS as the binder and cured under ambient conditions, exhibited 6% greater results than PCC, with similar compressive strength at 28 days [152]. However, as the proportion of FA substituting GGBFS increased from 0 to 70%, the splitting tensile strength decreased from 6.4 to 4.7 MPa at 28 days under ambient curing conditions. This is attributed to the decrease in calcium oxide and increase in silicon dioxide contents in the concrete matrix that occurred as FA amount increased [153].

A certain decrease in splitting tensile strength of 21% was observed by Bezemer et al. [41] for GGBFS-based and blended GGBFS/FA-based AAC, with no such reduction for the control PCC.

The research study conducted by Lee and Lee [112] compared the measured splitting tensile strength results of FA/GGBFS-based AAC with the predicted splitting tensile strength of PCC according to the ACI 318-08 code [154] and Eurocode 2 [128] (see Fig. 12).

The average splitting tensile strength can be calculated using Eq. (1) as outlined in [154]. Based on the findings by Lee and Lee [112], the following prediction equation for the splitting tensile strength of alkali-activated fly ash/slag concrete has been proposed (see Eq. 2):

$$f_{ct} = 0.56 \times \sqrt{f'_c} \tag{1}$$

$$f_{ct} = 0.45 \times \sqrt{f'_c} \tag{2}$$

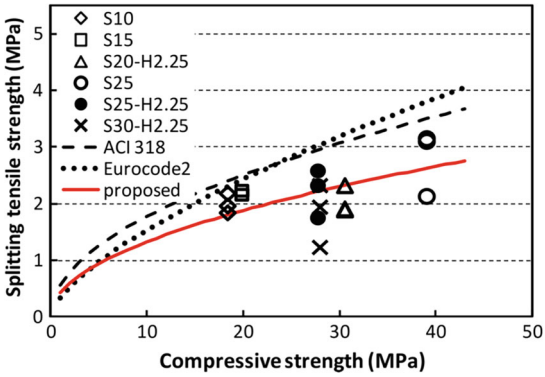

Fig. 12 Comparison of measured splitting tensile strength results with standard codes [112]

where f_{ct} is the splitting tensile strength, and f_c' is the compressive strength.

On the contrary, AAC produced with GGBFS as the sole binder, activated with calcium hydroxide [129] and a combination of sodium silicate and sodium hydroxide [118], exhibited splitting tensile strength that closely aligned with the predictions outlined in the ACI building code 318 [154]. In addition, when increasing GGBFS content, corresponding rise in the splitting tensile strength is observed [155].

Furthermore, several studies have revealed that the addition of nanomaterials into AAC leads to enhanced mechanical properties owing to the mechanism of nano-filling effect, providing nucleation sites for hydration, and crack-bridging [156]. Adak et al. [157] observed the effect of nano-silica on strength and durability characteristics of AAC, concluding that the inclusion of 56% nano-silica enhanced AAC splitting tensile strength under normal curing conditions. It was reported that compressive, splitting tensile, and flexural strengths increased with the addition of 6% nano-silica under ambient curing conditions. Furthermore, the incorporation of nano alumina into AAC enhanced the splitting tensile strength, irrespective of the type of binder used [158]. The addition of 0.1%, 0.5% and 1% graphene into FA/GGBFS-based AACs led to a 37%, 41% and 37% enhancement in splitting tensile strength, respectively. This enhancement is attributed to the densification of the microstructure in AAC resulting from the addition of graphene [159].

Rossi et al. [48] investigated the correlation between compressive strength and splitting tensile strength of different alkali-activated systems. Both splitting tensile and flexural strengths' results have been considered and analyzed. Similar to the findings observed for the elastic modulus, the correlation between compressive strength and indirect tensile strength is directly correlated to the type of binder used (Fig. 13).

While GGBFS-based AAC generally shows higher 28-day compressive strength values, it also tends to show higher splitting tensile strength, which is often underestimated by the current design codes and standards. However, it disagrees with the earlier statement by Rossi et al. [48]. Although several authors [42, 49, 112, 129, 160] proposed different analytical equations to predict the splitting tensile response of AACs, these correlations were derived from a limited amount of data points,

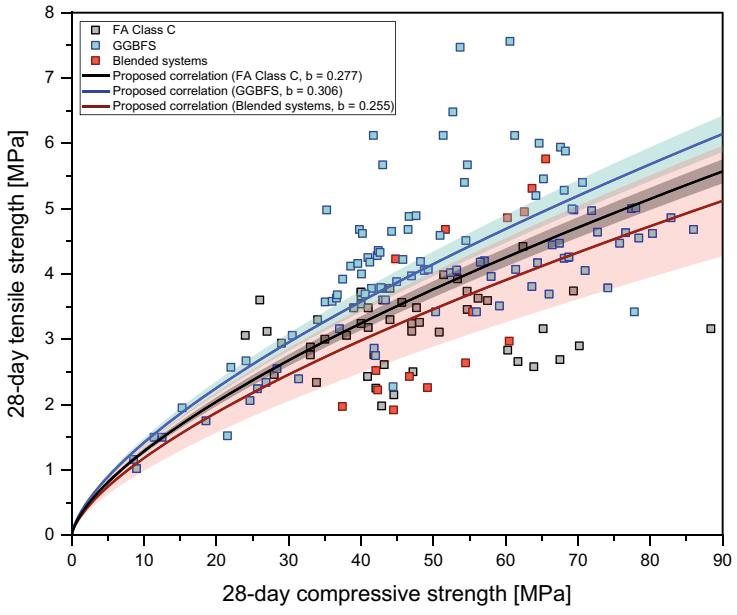

(a)

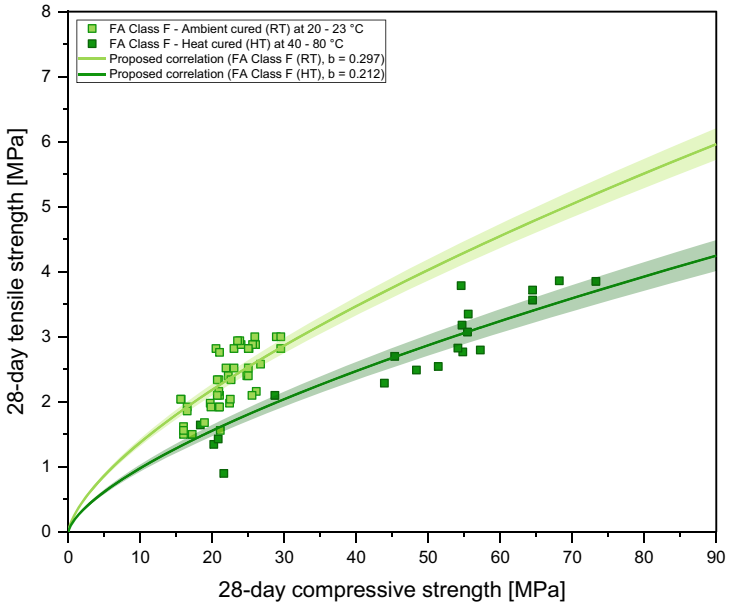

(b)

Fig. 13 Correlation between compressive strength and splitting tensile strength of different AACs, **a** high-calcium and **b** low-calcium [48]

making them dependent on AAC mix design. The study of Rossi et al. [48] demonstrated that the type of binder is not sufficient to fully characterize the variety of possible achievable AAC properties, as inside each alkali-activated system a wide scatter of mechanical behavior can be observed (Fig. 13a). Figure 13b shows that curing conditions affect the compressive-to-tensile strength relationship in low-calcium systems. Heat curing promotes rapid alkali activation process, forming a denser and more homogeneous matrix, which leads to a relatively higher increase in compressive strength. However, rapid setting can introduce microcracks and internal stresses, limiting tensile strength development. In contrast, ambient curing involves slower reaction rates, often resulting in lower overall compressive strength. Yet, the slower setting can reduce autogenous shrinkage-induced microcracks, so the relative increase in tensile strength can be more proportional to compressive strength compared to heat curing.

Some studies have adopted linear regression techniques to predict compressive strength as a function of the binder characteristics and the ultrasonic pulse velocity as presented in Eq. (3) [161]. It is important to note that these relationships are based on limited data and are empirical, lacking a clear understanding of the underlying mechanisms. Given the wide variety of AAC mixes and raw materials (e.g. incinerated bottom ashes), the efficiency of developing new empirical equations is uncertain. For example, in PCC, such equations took decades to develop. The correlation between the experimental and predicted values of splitting tensile and compressive strength as per different codal provisions, and along with comparison with the data from previous studies, is shown in Fig. 14. Additionally, another study has adopted non-linear regression to express the splitting tensile strength and modulus of rupture of blended AACs as a function of compressive strength, as presented in Eqs. (4) and (5), respectively [162]. The final expressions were analogous to the corresponding expressions for traditional PCC. However, both these approaches reported several uncertainties in the input parameters, indicating the need for further investigations necessary to improve the accuracy of these predictions.

$$f_c' = -4.535\vartheta_{(f,AAB)} + 13.852\vartheta_{(f,CASH)} + 18.264\vartheta - 55.323 \tag{3}$$

where f_c' is the compressive strength of AAC in MPa; $\vartheta_{(f,ABB)}$ is the volume fraction of reacted AAB paste products at any given degree of reaction; $\vartheta_{(f,CASH)}$ is the volume fraction of C–A–S–H at degree of slag hydration α (microstructural properties); ϑ is the result obtained from the ultrasonic pulse velocity test at specimen level in km/s.

$$f_t' = 0.0975 f_c' + 0.1259054 \tag{4}$$

$$f_r' = 0.639\sqrt{f_c'} \tag{5}$$

where, f_t' is the splitting tensile strength in MPa, f_r' is the modulus of rupture in MPa, and f_c' is the compressive strength of AAC in MPa.

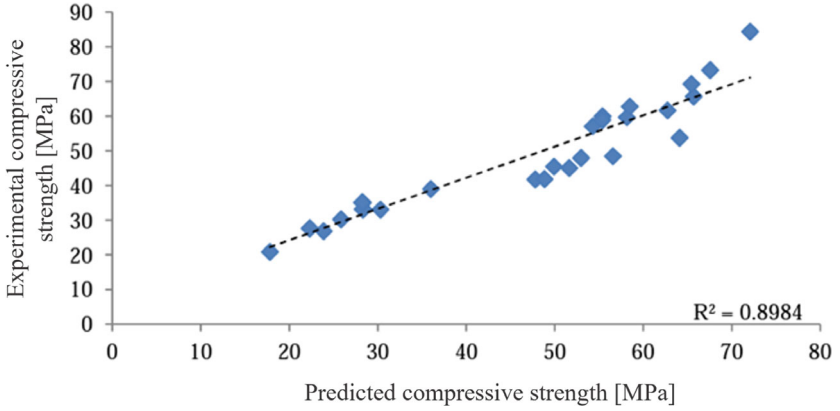

Fig. 14 Comparison between the predicted compressive strength and experimental values [161]

3.3 Elastic Modulus

Several studies have reported experimental data related to elastic modulus measurement following the American standard ASTM C469/C469M [163], but also following equivalent procedures as outlined in the International ISO 1920-10:2010 [164], the Australian AS 1012.17-1997 [165] and the British BS 1881-121:1983 [166] standards.

In case of standard PCC, empiric formulae are typically applied to establish a correlation between elastic modulus and compressive strength. However, as most studies report elastic modulus values lower than those of PCC, the accuracy of these conventional PCC models is limited for AAC [43, 152, 167, 168]. To address this issue, some authors have proposed more precise correlation models to predict AAC elastic modulus. However, all reported data are quite scattered, primarily dependent on the applied precursors, activators, aggregates (siliceous or limestone), mix design, and curing regime. As a result, there is no agreement among the different data.

In particular, Collins and Sanjayan [38] found that the elastic modulus of GGBFS-based AAC with the use of different alkali activators was marginally lower than that of PCC. Similarly, a 20–30% reduction in elastic modulus was observed for GGBFS-based and blended FA/GGBFS-based AAC over time by Bezemer et al. [41]. Douglas et al. [169] stated that the elastic modulus of AAC can be estimated from the corresponding compressive strength following the guidelines outlined in the ACI building code 318 [170]. Similarly, Yang et al. [129] noted that the elastic modulus of GGBFS-based AAC activated by calcium hydroxide can also be approximately predicted by the ACI building code 318 [170]. However, while most studies indicate that the elastic modulus of AAC falls within the same 10–40 GPa range as PCC, there are significant differences in results.

For GGBFS-based AAC, the elastic modulus aligns with predictions from PCC codes. In contrast, for FA-based AAC and blended GGBFS/FA-based AAC, these

codes tend to overestimate the elastic modulus. This difference appears because the intrinsic elastic modulus of gels is lower for NA–S–H gels formed in alkali-activated FA than C–A–S–H gels formed in alkali-activated GGBFS [43].

Rossi et al. [48] investigated the correlation between compressive strength and elastic modulus using a wide range of data collected from the available literature. As shown in Fig. 15, the elastic modulus of AAC, regardless of the binder type, is generally also lower than that of PCC and tends to be overestimated by current available design codes such as the *fib* Model Code 2010 [124], Eurocode 2 [128] and ACI-363R.10 [171].

In contrast, Thomas and Peethamparan [42] reported that the modulus of elasticity of GGBFS-based AAC varied linearly with the compressive strength and found that the ACI building code 318 [170] fitted reasonably well despite wide variation in data.

Nath and Sarker [125] investigated the influence of the curing regime on low-Ca FA-based AAC blended with GGBFS, PC and calcium hydroxide as additional calcium sources. It was found that curing at the room temperature, even if some delay in strength development occurs, led to similar elastic modulus values compared to high-temperature curing (<100 °C) at the same curing times. Considering both the curing regime, lower elastic modulus values (approximately 25–30% less) were

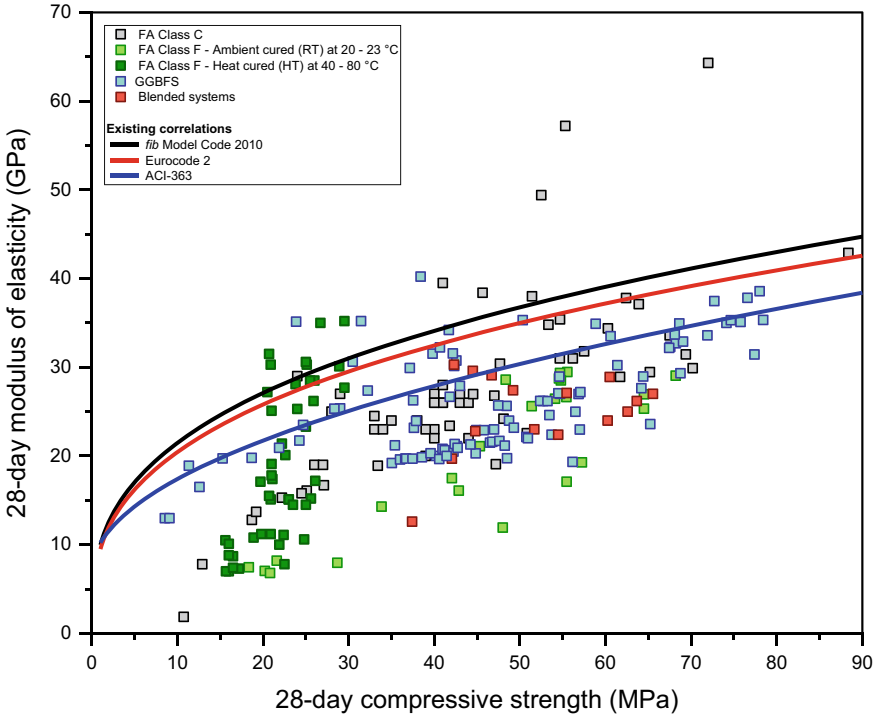

Fig. 15 Correlation between compressive strength and elastic modulus of different AACs [48]

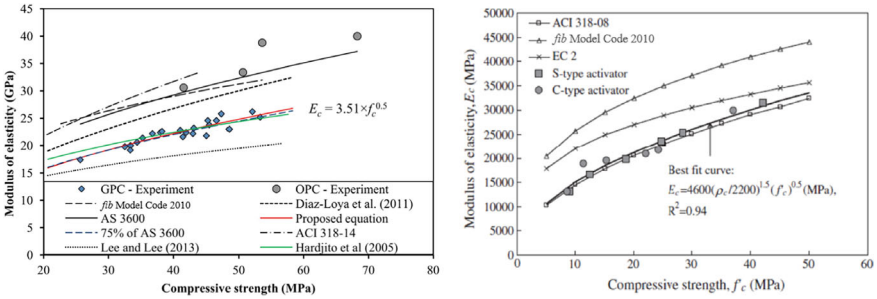

Fig. 16 Correlation between elastic modulus and compressive strength according to **a** Nath and Sarker [125], **b** Yang et al. [129]

measured compared to PCC and all predictive equations (as reported in AS 3600-2009, ACI 318-14 and the *fib* Model Code 2010) overestimated the elastic modulus value for AAC. For this reason, the authors proposed the following equation: $E_c = 3.51 \cdot f_c^{0.5}$, where f_c is the compressive strength of AAC in MPa, obtained from a regression analysis based on the experimental data, as depicted in Fig. 14.

Although Nath and Sarker [125] demonstrated that the elastic modulus of low-calcium systems AAC is usually lower than of PCC and, therefore, it is overestimated by most available standards, which are based on only a limited amount of data. Besides Nath and Sarker [125], different authors [129, 168] have proposed empirical relations between the compressive strength and the elastic modulus (see Fig. 16). Nevertheless, these equations are not universally applicable to AAC due to variations of types of FA, mix compositions, curing conditions, and aggregate type.

As shown in Fig. 17, the elastic modulus exhibits variations according to the binder type, with FA class F showing the lowest values.

Other studies highlighted the positive influence of GGBFS addition on elastic modulus values for FA-based AAC [153, 172] and linked it to the increasing content of calcium in the AAC network, which promotes the formation of C–A–S–H gels. Li et al. [40] reported a higher elastic modulus for GGBFS-based AAC in comparison to FA/GGBFS-based AAC at an early age. After 7 days, a certain decrease was observed for GGBFS-based AAC, while FA/GGBFS-based AAC showed an increase in the elastic modulus over time.

Fahim Huseien et al. [153] reported that elastic modulus values (ranging from 22.8 to 27.0 GPa) are directly influenced by the binder's chemical composition: increasing FA replacement in GGBFS binder induces a drop in elastic modulus values (up to 15% decrease with 30 wt.% of FA). In line with this, Aiken et al. [172] obtained elastic modulus values ranging from 21.1 to 28.9 GPa for FA-based AAC with a maximum GGBFS replacement of 30 wt.%, which led to an increase of 37% in the elastic modulus [172].

Prinsse et al. [37] reported on the elastic modulus performance in 100 wt.% GGBFS-based AAC and 50 wt.% FA/GGBFS-based AAC up to 2 years when

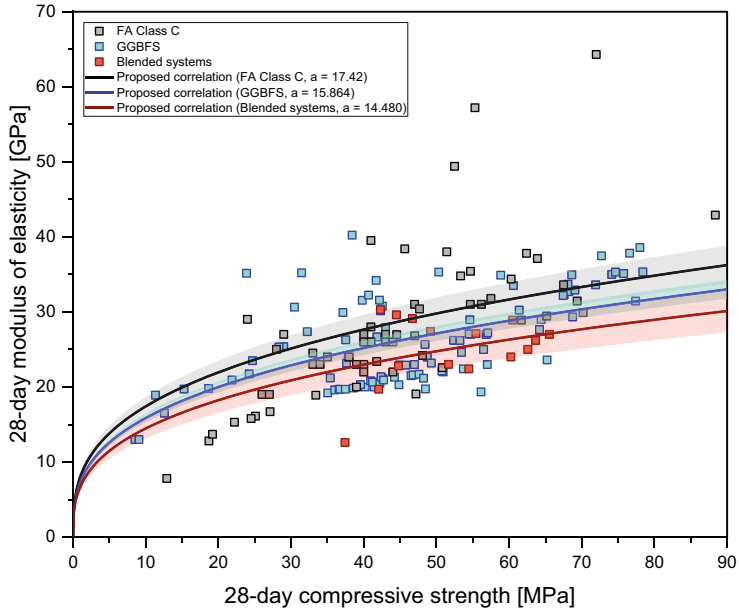

(a)

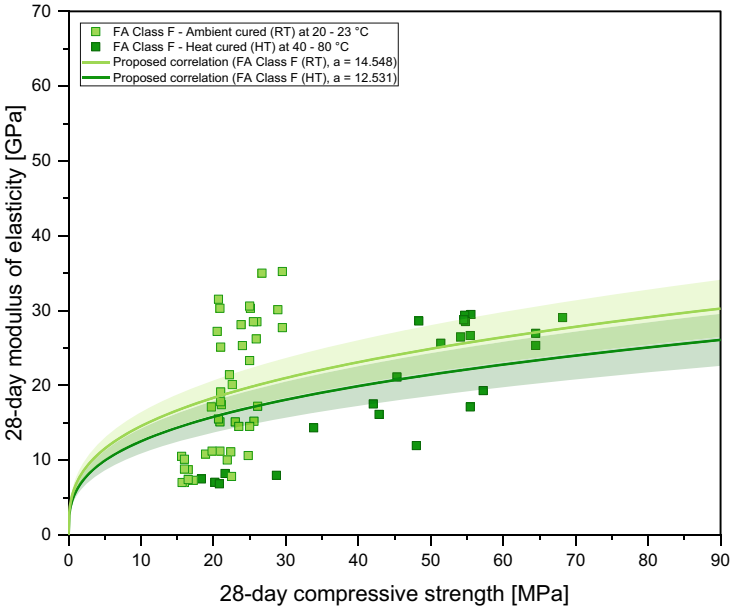

(b)

Fig. 17 New proposed correlations between compressive strength and elastic modulus of high-calcium (**a**) and low-calcium (**b**) systems [48]

exposed to drying. Later, this study was extended by Bezemer et al. [41] up to 5 years and then control PCCs were also included. At 28 days, elastic modulus values were 26.4 and 32.9 GPa for 50% and 100% GGBFS-based mixes, respectively. In [41] the reduction in elastic modulus observed in the blended GGBFS/FA-based AAC are linked to carbonation, which decalcifies the gels, increasing the binder's porosity and decreasing the elastic modulus. In contrast, carbonation in GGBFS-based AACs was minimal; instead, microcracking and C–A–S–H gel desiccation occurred during constant drying, which also contributed to the reduction in elastic modulus. The reported decrease was approximately 30% from 28 days to 5 years for the blended GGBFS/FA-based AAC and around 20% for the GGBFS-based AAC.

Wardhono et al. [39] observed the development of elastic modulus for GGBFS-based AAC and FA-based AAC between 28 and 540 days. The elastic modulus of FA-based AAC and GGBFS-based AAC ranged between 8–16 GPa and 26.8–15.3 GPa, respectively over the 28–540-day period. The FA-based AAC had a two-fold increase in elastic modulus from 28 to 540 days, while GGBFS-based AAC showed a 43% decrease during this time interval [39].

Najimi and Ghafoori [173] highlighted an increase in elastic modulus with increasing sodium silicate solution content and identified an optimum sodium hydroxide concentration that increases with increasing the GGBFS concentration in the GGBFS/natural pozzolan-based GGBFS. Aliabdo et al. [116] reported that increasing the sodium hydroxide molarity and the sodium silicate content led to a higher elastic modulus performance of GGBFS-based AAC.

3.4 Poisson's Ratio

Although several studies have reported Poisson's ratio of AAC, the results have been inconsistent. Albitar et al. [174] experimentally determined Poisson's ratio of FA-based AAC with an average value of 0.13. A similar average value of 0.14 for Poisson's ratio was determined by Hardjito and Rangan [175] and Diaz-Loya et al. [103]. Sun et al. [176], using machine learning algorithms, estimated the relationship between Poisson's ratio and compressive strength for binary GGBFS/FA-based AACs. It was observed that Poisson's ratio (ν) is identical to the one of PCC which is approximately 0.2 (see Fig. 18). Cong et al. [177] found that the Poisson's ratio of the GGBFS/FA-based AACs ranged from 0.205 to 0.257, significantly higher than the value of 0.149 observed for PCC.

While substantial progress has been accomplished in the assessment and comprehension of AAC mechanical properties, finding a generalized methodology to categorize these materials and establish a correlation between their mechanical performance and chemical composition (i.e., the binder type, the type and dosage of the alkaline solution, and long-term performance under exposure conditions play a crucial role) remains an ongoing pursuit. This includes sensitivity to carbonation and drying, along with their impact on the mechanical properties.

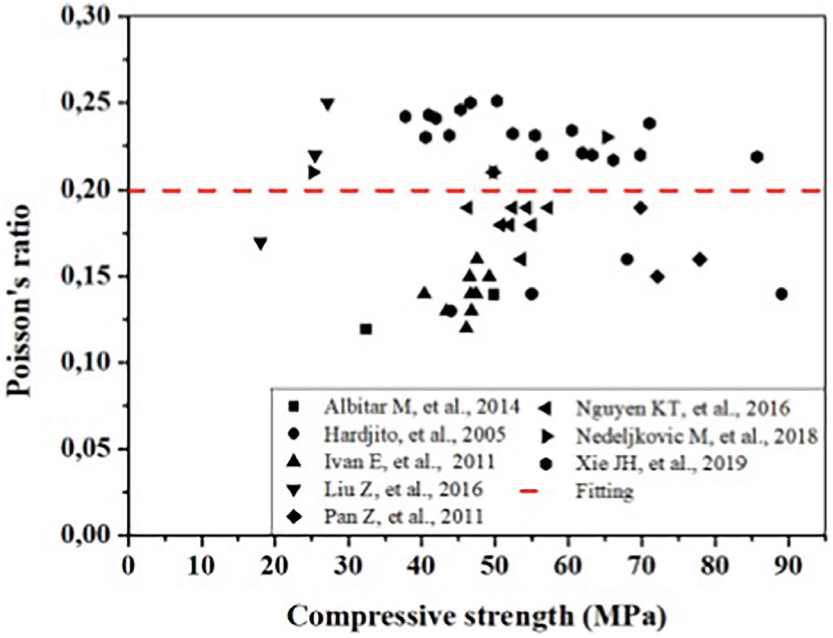

Fig. 18 Relationship between Poisson's ratio and compressive strength for GGBFS/FA-based AACs [176]

4 Conclusions

This chapter serves as a resource that highlights current knowledge and also identifies areas within the field requiring further exploration and research. Based on the state-of-the-art review of AAC past research carried out, the following can be concluded:

• AAC is considered as a replacement for PCC contingent upon a consistent and efficient supply of industrial waste materials for specific fields of application. However, this further justification is required, given the variability in mechanical properties, uncertainties in long-term performance, and the influence of testing methods.

• Extensive research has focused on evaluating the performance of common aluminosilicates, with particular emphasis on FA-based and GGBFS-based AAC due to their superior mechanical properties, attributed to their favorable physical and chemical characteristics among aluminosilicate-based AAMs.

• The mechanical properties of AAC are primarily influenced by their mix proportions. The complexity of AAC mix design arises from the manifold variables that impact the alkali-activation process, including alkali content, curing parameters (time and temperature), water-to-solid ratio, pH, activator molarity, raw material composition and type, activator, and silicate-to-hydroxide ratio. Current mix design procedures for AAC predominantly rely on empirical trial-and-error approaches.

• Previous investigations have evaluated the mechanical properties, considering different factors like NaOH/Na_2SiO_3 ratio, NaOH/GGBFS ratio, activator/binder ratio, the combination of different activators, curing conditions, curing temperature, curing duration, exposure to drying, ageing, exposure to carbonation, molarity of activators, different binders' ratio, and the addition of nanoparticles.

• GGBFS-based AAC can show relatively high early-age strength and quick development due to the rapid dissolution of GGBFS particles in alkaline conditions and the consequent rapid precipitation of reaction products.

• Typically, AAC exhibits lower flexural strength due to the limited presence of calcium essential for the formation of C–S–H and C–A–S–H. However, an increase in GGBFS content tends to enhance the splitting tensile strength. The introduction of co-binders, however, enhances splitting tensile and flexural strengths. Numerous studies corroborated that the incorporation of nanomaterials into AAC boosts mechanical properties through mechanisms like nano-filling effects, providing nucleation sites for hardening reaction, and crack-bridging.

• The elastic modulus data demonstrated substantial divergence, rendering that the utilization of proposed empirical correlations between compressive strength and elastic modulus formulation for PCC is inappropriate. Instead, the elastic modulus in AAC depends on the choice of precursor materials, activators, mix design parameters, and curing conditions.

5 Perspectives and Outlook

The current state-of-the-art review and contribution to an interlaboratory experimental investigation by RILEM TC 294-MPA RRT1 expert group [178] provided essential conclusions about the hardened AAC mechanical properties.

Despite being discovered a century ago, AAMs have not yet gained widespread acceptance in the construction industry in comparison to PCC due to several barriers and limitations. It is well-known that the rapid reaction in the early stage of AAC leads to a drastic reduction or even loss of workability and following mixing challenges. Admixtures and retarders are very crucial for application in AAC production technology, but unfortunately, they are often incompatible. There is a need for a novel method development that separates the application of admixtures and alkali activators in AAC production. Recently published RILEM TC 294-MPA Report [178] introduced the results of the reproducible GGBFS-based AAC mix design with an achieved target consistence class S4 and compressive strength above 55 MPa, and proved that AAC can be a good alternative to PCC.

An additional aspect to consider for further practical application of AAC in construction engineering is the constant development of mechanical properties over the long-term and exclusion of decreases in these properties. Even current AAC mix design approaches lead to improved AAC performance, curing conditions are crucially important for the development of hardened AAC properties.

Considering the increasing focus on zero CO_2 emission and intensive research, AAMs have gained spectacular attention in the last two decades. However, analyzing the variation in properties and establishing trends and connections from results obtained across various tools and disciplines might be challenging using traditional statistical approaches. Artificial Intelligence and Machine Learning show great potential for revealing hidden relationships and optimization design models for AAC [80, 179], enabling more sophisticated links across materials' properties.

Therefore, despite the solid knowledge developed during the last century of studying AAMs, certain aspects of the AAC require in-depth exploration from different perspectives to ensure their constant application in the construction industry.

Acknowledgements The authors would like to acknowledge the RILEM Technical Committee 294 Mechanical Properties of Alkali-Activated Concrete (TC 294-MPA) for providing the platform to conduct the review and obtain valuable insight on alkali-activated concrete. The authors would also like to thank their respective institutes, companies and organizations for providing the necessary resources to prepare this chapter.

Authors' Contributions All authors contributed to this paper. All authors read and approved the final manuscript of this chapter.

Conflicts of Interest The authors declare no conflict of interest.

References

1. Buchwald, A., Kaps, C., Hohmann, M.: Alkali-activated binders and pozzolan cement binders—Complete binder reaction or two sides of the same story? In: Proceedings of the 11th International Conference on the Chemistry of Cement, pp. 1238–1246, Durban, South Africa (2003)
2. Shi, C., Krivenko, P., Roy, D.: Alkali-Activated Cements and Concretes. CRC Press, London, UK (2003)
3. Provis, J.L., van Deventer, J.S.L.: Alkali Activated Materials. State-of-the-Art Report RILEM TC 224-AAM. Springer, Dordrecht, p. 388 (2014). https://doi.org/10.1007/978-94-007-7672-2
4. Pol Segura, I., Ranjbar, N., Juul Damø, A., Skaarup Jensen, L., Canut, M., Arendt Jensen, P.: A review: alkali-activated cement and concrete production technologies available in the industry. Heliyon **9**(5), e15718 (2023). https://doi.org/10.1016/j.heliyon.2023.e15718
5. Miranda de Lima, L., Bernal Lopez, S., Huang, Y., Marsh, A.T.M., Adesanya, E.D., Lukkonen, T., Yliniemi, J., Ye, G., Provis, J.L.: Chapter 3. Conventional precursors and activators. In: Ye, G., Dehn, F. (eds.) Mechanical Properties of Alkali-Activated Concrete. RILEM State-of-the-Art Reports. Springer. https://doi.org/10.1007/978-3-032-07116-3_3
6. Krishnan, S., Adesanya, E.D., Chen, B., Yankwa Djobo, J.N., Huang, Y., Marsh, A.T.M., Nedeljkovic, M., Ye, G., Yliniemi, J., Yue, Z., Bernal Lopez, S.: Chapter 4. Non-conventional precursors and activators. In: Ye, G., Dehn, F. (eds.) Mechanical properties of alkali-activated concrete. RILEM State-of-the-Art Reports. Springer. https://doi.org/10.1007/978-3-032-07116-3_4
7. Xu, H., Provis, J.L., van Deventer, J.S.J., Krivenko, P.V.: Characterization of aged slag concretes. ACI Mater. J. **105**(2), 131–139 (2008). https://doi.org/10.14359/19753.
8. Patent US544706A, Manufacture of cement, United States Patent Office. Accessed 20 Aug. 1895. https://patents.google.com/patent/US544706

9. Kuhl, H.: Slag cement and process of making the same. US Patent 900939A (1908)
10. Krivenko, P.V.: Alkali-activated aluminosilicates: past, present and future. Chem. Listy **102**(2008), 273–277 (2008)
11. Pan, Z., Yang, N.: Updated review on AAM research in China. In: First International Conference on Advances in Chemically-Activated Materials, vol. 72, pp. 45–55, Jinan, China, RILEM Pro (2010)
12. Roy, D.M.: Alkali-activated cements opportunities and challenges. Cem. Concr. Res. **29**(2), 249–254 (1999). https://doi.org/10.1016/S0008-8846(98)00093-3
13. Pacheco-Torgal, F., Castro-Gomes, J., Jalali, S.: Alkali-activated binders: a review: Part 1. Historical background, terminology, reaction mechanisms and hydration products. Constr. Build. Mater. **22**(7), 1305–1314 (2008). https://doi.org/10.1016/j.conbuildmat.2007.10.015
14. Palomo, A., Krivenko, P., Garcia-Lodeiro, I., Kavalerova, E., Maltseva, O., Fernández-Jiménez, A.: A review on alkaline activation: new analytical perspectives. Materiales de Construcción **64**(315), e022 (2014). https://doi.org/10.3989/mc.2014.00314
15. Provis, J.L., Bernal, S.A.: Milestones in the analysis of alkali-activated binders. J. Sustain. Cem.-Based Mater. **4**(2), 74–84 (2015). https://doi.org/10.1080/21650373.2014.958599
16. Luukkonen, T., Abdollahnejad, Z., Yliniemi, J., Kinnunen, P., Illikainen, M.: One-part alkali-activated materials: a review. Cem. Concr. Res. **103**, 21–34 (2018). https://doi.org/10.1016/j.cemconres.2017.10.001
17. Provis, J.L.: Alkali-activated materials. Cem. Concr. Res. **114**, 40–48 (2018). https://doi.org/10.1016/j.cemconres.2017.02.009
18. Li, N., Shi, C., Zhang, Z., Zhu, D., Hwang, H.-J., Zhu, Y., Sun, T.: A mixture proportioning method for the development of performance-based alkali-activated slag-based concrete. Cem. Concr. Compos. **93**, 163–174 (2018). https://doi.org/10.1016/j.cemconcomp.2018.07.009
19. Almutairi, A.L., Tayeh, B.A., Adesina, A., Isleem, H.F., Zeyad, A.M.: Potential applications of geopolymer concrete in construction: a review. Case Stud Constr Mater **15**, e00733 (2021). https://doi.org/10.1016/j.cscm.2021.e00733
20. E-crete.: Info available. http://www.zeobond.com/products-e-crete.html
21. ANSTO.: Green geopolymer concretes for Australian construction industry (2023). https://www.ansto.gov.au/our-facilities/australian-synchrotron/case-studies/advanced-manufacturing/green-geopolymer-concretesANSTO
22. EXEGY.: Soletanche Bachy pours its first ultra-low carbon concrete foundation barrette. https://www.soletanche-bachy.com/en/news/exegy-by-soletanche-bachy-first-ultra-low-carbon-concrete-foundation-barrette
23. RAMAC.: https://ramacreadymix.nl/en/home/
24. Palomo, A.: Sustainable binders and new ways of construction. In: Proceedings of the 1st Symposium Knowledge Exchange for Young Scientists (KEYS), pp. 51–56, Dares Salaam Tanzania (2015). https://www.rilem.net/global/gene/link.php?doc_id=4659&fg=1
25. CEMFREE. https://www.cemfree.com/
26. CEMEX. https://www.cemex.co.uk/lower-carbon-concrete
27. BLOCKWALLS. https://blockwalls.co.uk/
28. VicRoads specifications—Section 703 General Concrete Paving—Superceded, Australian Standards, VicRoads (2018)
29. GB/T 29423-2012.: Alkali-activated slag-fly ash concrete for anticorrosive cement products. General Administration of Quality Supervision, Inspection and Quarantine of the People's Republic of China, Standardization Administration of the People's Republic of China (2012)
30. IS 17452:2020.: Use of alkali activated concrete for precast products—Guidelines. Bureau of Indian Standards, New Delhi, India
31. SIA Merkblatt 2049:2014.: Anforderung an neue Zemente/Exigences relatives aux nouveaux ciments, Switzerland (2014)
32. DSTU B V.2.7-181.: Alkaline cements specifications. National Standard of Ukraine, Kiev (2009)
33. BSI Flex 350 v2.0:2024-09.: Alternative binder systems for lower carbon concrete—Code of practice. The British Standards Institution 2024, UK (2024)

34. PAS 8820:2016 Construction materials—Alkali-activated cementitious material and concrete—Specification. The British Standards Institution, UK (2016)
35. Collins, F., Sanjayan, J.G.: Microcracking and strength development of alkali activated slag concrete. Cem. Concr. Compos. **23**(4), 345–352 (2001). https://doi.org/10.1016/S0958-9465(01)00003-8
36. Un, C.H., Sanjayan, J.G., San Nicolas, R., van Deventer, J.S.J.: Predictions of long-term deflection of geopolymer concrete beams. Constr. Build. Mater. **94**, 10–19 (2015). https://doi.org/10.1016/j.conbuildmat.2015.06.030
37. Prinsse, S., Hordijk, D.A., Ye, G., Lagendijk, P., Luković, M.: Time-dependent material properties and reinforced beams behavior of two alkali-activated types of concrete. Struct. Concr. **21**(2), 642–658 (2020). https://doi.org/10.1002/suco.201900235
38. Collins, F.G., Sanjayan, J.G.: Workability and mechanical properties of alkali activated slag concrete. Cem. Concr. Res. **29**(3), 455–458 (1999). https://doi.org/10.1016/S0008-8846(98)00236-1
39. Wardhono, A., Gunasekara, C., Law, D.W., Setunge, S.: Comparison of long term performance between alkali activated slag and fly ash geopolymer concretes. Constr. Build. Mater. **143**, 272–279 (2017). https://doi.org/10.1016/j.conbuildmat.2017.03.153
40. Li, Z., Zhang, S., Liang, X., Ye, G.: Cracking potential of alkali-activated slag and fly ash concrete subjected to restrained autogenous shrinkage. Cem. Concr. Compos. **114**, 103767 (2020). https://doi.org/10.1016/j.cemconcomp.2020.103767
41. Bezemer, H.J., Awasthy, N., Luković, M.: Multiscale analysis of long-term mechanical and durability behaviour of two alkali-activated slag-based types of concrete. Constr. Build. Mater. **407**, 133507 (2023). https://doi.org/10.1016/j.conbuildmat.2023.133507
42. Thomas, R.J., Peethamparan, S.: Alkali-activated concrete: engineering properties and stress–strain behavior. Constr. Build. Mater. **93**, 49–56 (2015). https://doi.org/10.1016/j.conbuildmat.2015.04.039
43. Ding, Y., Dai, J.-G., Shi, C.-J.: Mechanical properties of alkali-activated concrete: a state-of-the-art review. Constr. Build. Mater. **127**, 68–79 (2016). https://doi.org/10.1016/j.conbuildmat.2016.09.121
44. Adesina, A.: Performance of fibre reinforced alkali-activated composites—A review. Materialia **12**, 100782 (2020). https://doi.org/10.1016/j.mtla.2020.100782
45. Ramagiri, K.K.: Evaluation of high-temperature, bond, and shrinkage of alkali-activated binder concrete. Ph.D. thesis. Birla Institute of Technology and Science, Pilani, India (2021)
46. Kirubajiny, P., Marita, B., Jay, S., Pathmanathan, R., Didar, S.C.: Durability performance of precast fly ash based geopolymer concrete under atmospheric exposure conditions. J. Mater. Civ. Eng. **30**(3), 04018007 (2018). https://doi.org/10.1061/(ASCE)MT.1943-5533.0002165
47. Jittin, V., Madhuri, P., Santhanam, M., Bahurudeen, A.: Influence of preconditioning and curing methods on the durability performance of alkali-activated binder composites. Constr. Build. Mater. **311**, 125346 (2021). https://doi.org/10.1016/j.conbuildmat.2021.125346
48. Rossi, L., Miranda de Lima, L., Sun, Y., Dehn, F., Provis, J.L., Ye, G., De Schutter, G.: Future perspectives for alkali-activated materials: from existing standards to structural applications. RILEM Tech. Lett. **7**, 159–177 (2022)
49. Xie, T., Visintin, P., Zhao, X., Gravina, R.: Mix design and mechanical properties of geopolymer and alkali activated concrete: review of the state-of-the-art and the development of a new unified approach. Constr. Build. Mater. **256**, 119380 (2020). https://doi.org/10.1016/j.conbuildmat.2020.119380
50. Cao, C.: Sustainability and life assessment of high strength natural fibre composites in construction. In: Advanced High Strength Natural Fibre Composites in Construction, pp. 529–544 (2017). https://doi.org/10.1016/B978-0-08-100411-1.00021-2
51. Cunningham, P.R., Miller, S.A.: Quantitative assessment of alkali-activated materials: environmental impact and property assessments. J. Infrastruct. Syst. **26**(3), 04020021 (2020). https://doi.org/10.1061/(ASCE)IS.1943-555X.0000556
52. Turner, L.K., Collins, F.G.: Carbon dioxide equivalent (CO2-e) emissions: a comparison between geopolymer and OPC cement concrete. Constr. Build. Mater. **43**, 125–130 (2013). https://doi.org/10.1016/j.conbuildmat.2013.01.023

53. Weil, M., Dombrowski, K., Buchwald, A.: Life-cycle analysis of geopolymers. In: Geopolymers, Structures, Processing, Properties and Industrial Applications, pp. 194–210. Woodhead Publishing Series in Civil and Structural Engineering (2009). https://doi.org/10.1533/9781845696382.2.194
54. EN 206:2013.: Concrete: specification, performance, production and conformity. European Committee for Standardization (CEN), Brussels, Belgium (2013)
55. DIN 1045-4:2012-02.: Concrete, reinforced and prestressed concrete structures—Part 4: additional rules for the production and the conformity of prefabricated elements. DIN Media GmbH, Berlin, Germany (2012)
56. Habert, G., d'Espinose de Lacaillerie, J.B., Roussel, N.: An environmental evaluation of geopolymer based concrete production: reviewing current research trends. J. Clean. Prod. **19**(11), 1229–1238 (2011). https://doi.org/10.1016/j.jclepro.2011.03.012
57. McLellan, B.C., Williams, R.P., Lay, J., van Riessen, A., Corder, G.D.: Costs and carbon emissions for geopolymer pastes in comparison to ordinary portland cement. J. Clean. Prod. **19**(9), 1080–1090 (2011). https://doi.org/10.1016/j.jclepro.2011.02.010
58. Yang, K.-H., Song, J.-K., Song, K.-I.: Assessment of CO2 reduction of alkali-activated concrete. J. Clean. Prod. **39**, 265–272 (2013). https://doi.org/10.1016/j.jclepro.2012.08.001
59. Jiang, M., Chen, X., Rajabipour, F., Hendrickson, C.T.: Comparative life cycle assessment of conventional, glass powder, and alkali-activated slag concrete and mortar. J. Infrastruct. Syst. **20**(4), 04014020 (2014). https://doi.org/10.1061/(ASCE)IS.1943-555X.0000211
60. Robayo-Salazar, R., Mejía-Arcila, J., Mejía de Gutiérrez, R., Martínez, E.: Life cycle assessment (LCA) of an alkali-activated binary concrete based on natural volcanic pozzolan: a comparative analysis to OPC concrete. Constr. Build. Mater. **176**, 103–111 (2018). https://doi.org/10.1016/j.conbuildmat.2018.05.017
61. Fořt, J., Vejmelková, E., Koňáková, D., Alblová, N., Čáchová, M., Keppert, M., Rovnaníková, P., Černý, R.: Application of waste brick powder in alkali activated aluminosilicates: functional and environmental aspects. J. Clean. Prod. **194**, 714–725 (2018). https://doi.org/10.1016/j.jclepro.2018.05.181
62. Adesanya, E., Ohenoja, K., Di Maria, A., Kinnunen, P., Illikainen, M.: Alternative alkali-activator from steel-making waste for one-part alkali-activated slag. J. Clean. Prod. **274**, 123020 (2020). https://doi.org/10.1016/j.jclepro.2020.123020
63. Abdulkareem, M., Havukainen, J., Horttanainen, M.: How environmentally sustainable are fibre reinforced alkali-activated concretes? J. Clean. Prod. **236**, 117601 (2019). https://doi.org/10.1016/j.jclepro.2019.07.076
64. Bajpai, R., Choudhary, K., Srivastava, A., Sangwan, K.S., Singh, M.: Environmental impact assessment of fly ash and silica fume based geopolymer concrete. J. Clean. Prod. **254**, 120147 (2020). https://doi.org/10.1016/j.jclepro.2020.120147
65. Ramagiri, K.K., Chintha, R., Bandlamudi, R.K., Kara De Maeijer, P., Kar, A.: Cradle-to-gate life cycle and economic assessment of sustainable concrete mixes - alkali-activated concrete (AAC) and bacterial concrete (BC). Infrastructures **6**(7), 104 (2021). https://doi.org/10.3390/infrastructures6070104
66. Abdulkareem, M., Havukainen, J., Nuortila-Jokinen, J., Horttanainen, M.: Environmental and economic perspective of waste-derived activators on alkali-activated mortars. J. Clean. Prod. **280**, 124651 (2021). https://doi.org/10.1016/j.jclepro.2020.124651
67. Fernando, S., Gunasekara, C., Law, D.W., Nasvi, M.C.M., Setunge, S., Dissanayake, R.: Life cycle assessment and cost analysis of fly ash–rice husk ash blended alkali-activated concrete. J. Environ. Manag. **295**, 113140 (2021). https://doi.org/10.1016/j.jenvman.2021.113140
68. ISO 14044:2006.: Environmental management—Life cycle assessment—Requirements and guidelines. International Standard Organization (2006)
69. EN 12390-3: Testing hardened concrete—Part 3: compressive strength of test specimens. European Committee for Standardization (CEN), Brussels, Belgium (2019)
70. ASTM C39/C39M-21.: Standard test method for compressive strength of cylindrical concrete specimens. American Society for Testing and Materials. West Conshohocken, PA, USA (2021)

71. ASTM C496/C496M-17.: Standard test method for splitting tensile strength of cylindrical concrete specimens. American Society for Testing and Materials. West Conshohocken, PA, USA (2017)
72. EN 12390-6.: Testing hardened concrete part 6: tensile splitting strength of test specimens. European Committee for Standardization (CEN), Brussels, Belgium
73. ASTM C469/C469M-22.: Standard test method for static modulus of elasticity and poisson's ratio of concrete in compression. ASTM International, West Conshohocken, PA, USA
74. EN 12390-13.: Testing hardened concrete—Part 13: determination of secant modulus of elasticity in compression. European Committee for Standardization (CEN), Brussels, Belgium
75. Sun, Y., Dai, X., Sun, B., Attupurathu Vijayan, R., Tao, Y., Yliniemi, J., Gao, M., Sha, W., Palacios, M., Puertas Maroto, F., De Schutter, G.: Chapter 6. Fresh AAM properties. In: Ye, G., Dehn, F. (eds.) Mechanical Properties of Alkali-Activated Concrete. RILEM State-of-the-Art Reports. Springer. https://doi.org/10.1007/978-3-032-07116-3_6
76. Li, N., Shi, C., Zhang, Z., Wang, H., Liu, Y.: A review on mixture design methods for geopolymer concrete. Compos. B Eng. **178**, 107490 (2019). https://doi.org/10.1016/j.compositesb.2019.107490
77. IS 10262-2019.: Indian standard concrete mix proportioning—Guidelines (Second Revision). Bureau of Indian Standards, New Delhi, India
78. BSI-5328:1997 (Part 2).: Methods for specifying concrete mixes. British Standard, London, UK
79. ACI 211.1-91 (Reapproved 2002).: Standard practice for selecting proportions for normal, heavy weight, and mass concrete. Reported by ACI Committee 211
80. Völker, C., Moreno Torres, B., Rug, T., Firdous, R., Jan Zia, G.A., Lüders, S., Scaffino, H.L., Höpler, M., Böhmer, F., Pfaff, M., Stephan, D., Kruschwitz, S.: Data driven design of alkali-activated concrete using sequential learning. J. Clean. Prod. **418**, 138221 (2023). https://doi.org/10.1016/j.jclepro.2023.138221
81. Nazari, A., Khanmohammadi, H., Amini, M., Hajiallahyari, H., Rahimi, A.: Production geopolymers by Portland cement: designing the main parameters' effects on compressive strength by Taguchi method. Mater. Des. **41**, 43–49 (2012). https://doi.org/10.1016/j.matdes.2012.04.045
82. Patankar, S.V., Ghugal, Y.M., Jamkar, S.S.: Effect of concentration of sodium hydroxide and degree of heat curing on fly ash-based geopolymer mortar. Indian J. Eng. Mater. Sci. **2014**, 938789 (2014). https://doi.org/10.1155/2014/938789
83. Patil, A.A., Chore, H.S., Dodeb, P.A.: Effect of curing condition on strength of geopolymer concrete. Adv. Concr. Constr. **2**(1), 29–37 (2014). https://doi.org/10.12989/ACC.2014.2.1.029
84. Ferdous, M., Kayali, O., Khennane, A.: A detailed procedure of mix design for fly ash based geopolymer concrete. In: Proceedings of the Fourth Asia-Pacific Conference on FRP in Structures (APFIS 2013), pp. 11–13, Melbourne, Australia (2013). https://researchbank.swinburne.edu.au/file/552b44c9-7cb9-4509-8229-ec0f1f9bba0c/1/PDF%20%28Published%20version%29.pdf
85. Al Bakri, A.M., Kamarudin, H., Bnhussain, M., Nizar, I.K., Mastura, W.: Mechanism and chemical reaction of fly ash geopolymer cement—A review. Asian J. Sci. Res. **1**(5), 247–253 (2011)
86. Gunasekara, M., Law, D., Setunge, S.: Effect of composition of fly ash on compressive strength of fly ash based geopolymer mortar. In: Proceedings of the 23rd Australasian Conference on the Mechanics of Structures and Materials (ACMSM23), Byron Bay, Australia (2014)
87. Duxson, P., Mallicoat, S.W., Lukey, G.C., Kriven, W.M., van Deventer, J.S.J.: The effect of alkali and Si/Al ratio on the development of mechanical properties of metakaolin-based geopolymers. Coll Surf. A: Physicochem. Eng. Asp. **292**(1), 8–20 (2007). https://doi.org/10.1016/j.colsurfa.2006.05.044
88. Pavithra, P., Srinivasula Reddy, M., Dinakar, P., Hanumantha Rao, B., Satpathy, B., Mohanty, A.: Effect of the Na2SiO3/NaOH ratio and NaOH molarity on the synthesis of fly ash-based geopolymer mortar. In: Geo-Chicago, pp. 336–344 (2016). https://doi.org/10.1061/9780784480151.034

89. Gopalakrishna, B., Dinakar, P.: Mix design development of fly ash-GGBS based recycled aggregate geopolymer concrete. J. Build. Eng. **63**, 105551 (2023). https://doi.org/10.1016/j.jobe.2022.105551
90. Bondar, D., Nanukuttan, S., Provis, J.L., Soutsos, M.: Efficient mix design of alkali activated slag concretes based on packing fraction of ingredients and paste thickness. J. Clean. Prod. **218**, 438–449 (2019). https://doi.org/10.1016/j.jclepro.2019.01.332
91. Najm, O., El-Hassan, H., El-Dieb, A.: Optimization of alkali-activated ladle slag composites mix design using taguchi-based TOPSIS method. Constr. Build. Mater. **327**, 126946 (2022). https://doi.org/10.1016/j.conbuildmat.2022.126946
92. Xie, T., Zhao, X.: A mix-design procedure for alkali-activated concrete based on the concept of reactive modulus. In: Pacheco-Torgal, F., Chindaprasirt, P., Ozbakkaloglu, T. (eds.), Handbook of Advances in Alkali-Activated Concrete, pp. 15–40. Woodhead Publishing (2022). https://doi.org/10.1016/B978-0-323-85469-6.00016-7
93. 211.4R-93.: Guide for Selecting Proportions for High-Strength Concrete with Portland Cement and Fly Ash (Reapproved 1998), American Concrete Institute
94. Phoo-Ngernkham, T., Phiangphimai, C., Damrongwiriyanupap, N., Hanjitsuwan, S., Thumrongvut, J., Chindaprasirt, P.: A mix design procedure for alkali-activated high-calcium fly ash concrete cured at ambient temperature. Adv. Mater. Sci. Eng. **2460403**, 1–13 (2018). https://doi.org/10.1155/2018/2460403
95. Rafeet, A., Vinai, R., Soutsos, M., Sha, W.: Guidelines for mix proportioning of fly ash/GGBS based alkali activated concretes. Constr. Build. Mater. **147**, 130–142 (2017). https://doi.org/10.1016/j.conbuildmat.2017.04.036
96. Taguchi, G.C.S.W.Y.: Taguchi's Quality Engineering Handbook. Wiley-Interscience (2004)
97. Riahi, S., Nazari, A., Zaarei, D., Khalaj, G., Bohlooli, H., Kaykha, M.M.: Compressive strength of ash-based geopolymers at early ages designed by Taguchi method. Mater. Des. **37**, 443–449 (2012). https://doi.org/10.1016/j.matdes.2012.01.030
98. Olivia, M., Nikraz, H.: Properties of fly ash geopolymer concrete designed by Taguchi method. Mater. Des. (1980–2015), **36**, 191–198 (2012). https://doi.org/10.1016/j.matdes.2011.10.036
99. Hadi, M.N.S., Farhan, N.A., Sheikh, M.N.: Design of geopolymer concrete with GGBFS at ambient curing condition using Taguchi method. Constr. Build. Mater. **140**, 424–431 (2017). https://doi.org/10.1016/j.conbuildmat.2017.02.131
100. Rangan, B.V.: Concrete Construction Engineering Handbook. CRC Press, New York (2007)
101. Kong, D.L.Y., Sanjayan, J.G.: Damage behavior of geopolymer composites exposed to elevated temperatures. Cem. Concr. Compos. **30**(10), 986–991 (2008). https://doi.org/10.1016/j.cemconcomp.2008.08.001
102. Diaz-Loya, E.I., Allouche, E.N., Eklund, S.: Factors affecting the suitability of fly ash as source material for geopolymers. Fuel **89**(5), 992–996 (2010). https://doi.org/10.1016/j.fuel.2009.09.012
103. Diaz-Loya, E.I., Allouche, E.N., Vaidya, S.: Mechanical properties of fly-ash-based geopolymer concrete. ACI Mater. J. **108**(3), 300–306 (2011). https://doi.org/10.14359/51682495
104. Talha Junaid, M., Kayali, O., Khennane, A., Black, J.: A mix design procedure for low calcium alkali activated fly ash-based concretes. Constr. Build. Mater. **79**, 301–310 (2015). https://doi.org/10.1016/j.conbuildmat.2015.01.048
105. Sun, B., Sun, Y., Ye, G., De Schutter, G.: A mix design methodology of blast furnace slag and fly ash-based alkali-activated concrete. Cem. Concr. Compos. **140**, 105076 (2023). https://doi.org/10.1016/j.cemconcomp.2023.105076
106. Nath, P., Sarker, P.K.: Effect of GGBFS on setting, workability and early strength properties of fly ash geopolymer concrete cured in ambient condition. Constr. Build. Mater. **66**, 163–171 (2014). https://doi.org/10.1016/j.conbuildmat.2014.05.080
107. Gao, X., Yu, Q.L., Brouwers, H.J.H.: Reaction kinetics, gel character and strength of ambient temperature cured alkali activated slag–fly ash blends. Constr. Build. Mater. **80**, 105–115 (2015). https://doi.org/10.1016/j.conbuildmat.2015.01.065

108. Bakharev, T., Sanjayan, J.G., Cheng, Y.B.: Effect of admixtures on properties of alkali-activated slag concrete. Cem. Concr. Res. **30**(9), 1367–1374 (2000). https://doi.org/10.1016/S0008-8846(00)00349-5
109. Tong, S., Yuqi, Z., Qiang, W.: Recent advances in chemical admixtures for improving the workability of alkali-activated slag-based material systems. Constr. Build. Mater. **272**, 121647 (2021). https://doi.org/10.1016/j.conbuildmat.2020.121647
110. Li, N., Shi, C., Wang, Q., Zhang, Z., Ou, Z.: Composition design and performance of alkali-activated cements. Mater. Struct. **50**(3), 178 (2017). https://doi.org/10.1617/s11527-017-1048-0
111. Puertas, F., Varga, C., Alonso, M.M.: Rheology of alkali-activated slag pastes. Effect of the nature and concentration of the activating solution. Cem. Concr. Compos. **53**, 279–288 (2014). https://doi.org/10.1016/j.cemconcomp.2014.07.012
112. Lee, N.K., Lee, H.K.: Setting and mechanical properties of alkali-activated fly ash/slag concrete manufactured at room temperature. Constr. Build. Mater. **47**, 1201–1209 (2013). https://doi.org/10.1016/j.conbuildmat.2013.05.107
113. Palomo, A., Grutzeck, M.W., Blanco, M.T.: Alkali-activated fly ashes: a cement for the future. Cem. Concr. Res. **29**(8), 1323–1329 (1999). https://doi.org/10.1016/S0008-8846(98)00243-9
114. Ishwarya, G., Singh, B., Deshwal, S., Bhattacharyya, S.K.: Effect of sodium carbonate/sodium silicate activator on the rheology, geopolymerization and strength of fly ash/slag geopolymer pastes. Cem. Concr. Compos. **97**, 226–238 (2019). https://doi.org/10.1016/j.cemconcomp.2018.12.007
115. Bakharev, T., Sanjayan, J.G., Cheng, Y.B.: Effect of elevated temperature curing on properties of alkali-activated slag concrete. Cem. Concr. Res. **29**(10), 1619–1625 (1999). https://doi.org/10.1016/S0008-8846(99)00143-X
116. Aliabdo, A.A., Abd Elmoaty, A.E.M., Emam, M.A.: Factors affecting the mechanical properties of alkali activated ground granulated blast furnace slag concrete. Constr. Build. Mater. **197**, 339–355 (2019). https://doi.org/10.1016/j.conbuildmat.2018.11.086
117. Memon, F.A., Nuruddin, M.F., Demie, S., Shafiq, N.: Effect of curing conditions on strength of fly ash-based self-compacting geopolymer concrete. Int. J. Environ. Eng. **5**(8), 342–345 (2011). https://doi.org/10.5281/zenodo.1070949
118. Chi, M.: Effects of dosage of alkali-activated solution and curing conditions on the properties and durability of alkali-activated slag concrete. Constr. Build. Mater. **35**, 240–245 (2012). https://doi.org/10.1016/j.conbuildmat.2012.04.005
119. Tran, T.T., Kang, H., Kwon, H.-M.: Effect of heat curing method on the mechanical strength of alkali-activated slag mortar after high-temperature exposure. Materials **12**(11), 1789 (2019). https://doi.org/10.3390/ma12111789
120. Humad, A.M., Provis, J.L., Habermehl-Cwirzen, K., Rajczakowska, M., Ćwirzeń, A.: Creep and long-term properties of alkali-activated Swedish-slag concrete. J. Mater. Civ. Eng. (2021). https://doi.org/10.1061/(ASCE)MT.1943-5533.000338
121. Li, Z., Delsaute, B., Lu, T., Kostiuchenko, A., Staquet, S., Ye, G.: A comparative study on the mechanical properties, autogenous shrinkage and cracking proneness of alkali-activated concrete and ordinary Portland cement concrete. Constr. Build. Mater. **292**, 123418 (2021). https://doi.org/10.1016/j.conbuildmat.2021.123418
122. Li, Z., Lu, T., Liang, X., Dong, H., Ye, G.: Mechanisms of autogenous shrinkage of alkali-activated slag and fly ash pastes. Cem. Concr. Res. **135**, 106107 (2020). https://doi.org/10.1016/j.cemconres.2020.106107
123. Ma, J., Dehn, F.: Shrinkage and creep behavior of an alkali-activated slag concrete. Struct. Concr. **18**(5), 801–810 (2017). https://doi.org/10.1002/suco.201600147
124. CEB/fib.: Model Code 2010—Final draft, Volume 2. fib Bulletin No. 66, Ernst & Sohn (2012)
125. Nath, P., Sarker, P.K.: Flexural strength and elastic modulus of ambient-cured blended low-calcium fly ash geopolymer concrete. Constr. Build. Mater. **130**, 22–31 (2017). https://doi.org/10.1016/j.conbuildmat.2016.11.034
126. Ye, H., Radlińska, A.: Shrinkage mechanisms of alkali-activated slag. Cem. Concr. Res. **88**, 126–135 (2016). https://doi.org/10.1016/j.cemconres.2016.07.001

127. Castel, A., Foster, S.J., Ng, T., Sanjayan, J.G., Gilbert, R.I.: Creep and drying shrinkage of a blended slag and low calcium fly ash geopolymer concrete. Mater. Struct. **49**(5), 1619–1628 (2016). https://doi.org/10.1617/s11527-015-0599-1
128. EN 1992-1-1:2005/A1:2015.: Eurocode 2: Design of concrete structures—Part 1-1: general rules and rules for buildings. European Committee for Standardization (CEN), Brussels, Belgium
129. Yang, K.-H., Cho, A.-R., Song, J.-K.: Effect of water–binder ratio on the mechanical properties of calcium hydroxide-based alkali-activated slag concrete. Constr. Build. Mater. **29**, 504–511 (2012). https://doi.org/10.1016/j.conbuildmat.2011.10.062
130. Parthiban, K., Saravanarajamohan, K., Shobana, S., Anchal Bhaskar, A.: Effect of replacement of slag on the mechanical properties of fly ash based geopolymer concrete. Int. J. Eng. Sci. Technol. **5**(3), 2555–2559 (2013)
131. Sofi, M., van Deventer, J.S.J., Mendis, P.A., Lukey, G.C.: Engineering properties of inorganic polymer concretes (IPCs). Cem. Concr. Res. **37**(2), 251–257 (2007). https://doi.org/10.1016/j.cemconres.2006.10.008
132. Puertas, F., Martínez-Ramírez, S., Alonso, S., Vázquez, T.: Alkali-activated fly ash/slag cements: strength behaviour and hydration products. Cem. Concr. Res. **30**(10): 1625–1632 (2000). https://doi.org/10.1016/S0008-8846(00)00298-2
133. Assi, L.N., Eddie Deaver, E., Ziehl, P.: Effect of source and particle size distribution on the mechanical and microstructural properties of fly ash-based geopolymer concrete. Constr. Build. Mater. **167**, 372–380 (2018). https://doi.org/10.1016/j.conbuildmat.2018.01.193
134. Islam, A., Alengaram, U.J., Jumaat, M.Z., Bashar, I.I.: The development of compressive strength of ground granulated blast furnace slag-palm oil fuel ash-fly ash based geopolymer mortar. Mater. Des. **1980–2015**(56), 833–841 (2014). https://doi.org/10.1016/j.matdes.2013.11.080
135. Ranjbar, N., Mehrali, M., Behnia, A., Alengaram, U.J., Jumaat, M.Z.: Compressive strength and microstructural analysis of fly ash/palm oil fuel ash based geopolymer mortar. Mater. Des. **59**, 532–539 (2014). https://doi.org/10.1016/j.matdes.2014.03.037
136. Vora, P.R., Dave, U.V.: Parametric studies on compressive strength of geopolymer concrete. Procedia Eng **51**, 210–219 (2013). https://doi.org/10.1016/j.proeng.2013.01.030
137. Elyamany, H.E., Abd Elmoaty, A.E.M., Elshaboury, A.M.: Setting time and 7-day strength of geopolymer mortar with various binders. Constr. Build. Mater. **187**, 974–983 (2018). https://doi.org/10.1016/j.conbuildmat.2018.08.025
138. Fernández-Jiménez, A., Palomo, J.G., Puertas, F.: Alkali-activated slag mortars: mechanical strength behaviour. Cem. Concr. Res. **29**(8), 1313–1321 (1999). https://doi.org/10.1016/S0008-8846(99)00154-4
139. Bernal, S.A., Mejía de Gutiérrez, R., Pedraza, A.L., Provis, J.L., Rodriguez, E.D., Delvasto, S.: Effect of binder content on the performance of alkali-activated slag concretes. Cem. Concr. Res. **41**(1), 1–8 (2011). https://doi.org/10.1016/j.cemconres.2010.08.017
140. Al-Otaibi, S.: Durability of concrete incorporating GGBS activated by water-glass. Constr. Build. Mater. **22**(10), 2059–2067 (2008). https://doi.org/10.1016/j.conbuildmat.2007.07.023
141. Mithun, B.M., Mattur, C.N.: Self-cured alkali activated slag concrete mixes—An experimental study. Int. J. Environ. Eng. **8**(4), 477–482 (2014). https://doi.org/10.5281/zenodo.1093468
142. Bilek, V., Hurta, J., Done, P., Zidek, L.: Development of alkali-activated concrete for structures—Mechanical properties and durability. Perspect. Sci. **7**, 190–194 (2016). https://doi.org/10.1016/j.pisc.2015.11.031
143. Sun, B., Ye, G., De Schutter, G.: A review: reaction mechanism and strength of slag and fly ash-based alkali-activated materials. Constr. Build. Mater. **326**, 126843 (2022). https://doi.org/10.1016/j.conbuildmat.2022.126843
144. ASTM C78/C78M-18.: Standard Test. Method for flexural strength of concrete (using simple beam with third-point loading); American Society for Testing and Materials: West Conshohocken, PA, USA (2018)
145. EN 12390-5:2019.: Testing hardened concrete. Flexural strength of test specimens. European Committee for Standardization (CEN), Brussels, Belgium

146. Yurt, Ü.: High performance cementless composites from alkali activated GGBFS. Constr. Build. Mater. **264**, 120222 (2020). https://doi.org/10.1016/j.conbuildmat.2020.120222
147. Deb, P.S., Nath, P., Sarker, P.K.: The effects of ground granulated blast-furnace slag blending with fly ash and activator content on the workability and strength properties of geopolymer concrete cured at ambient temperature. Mater. Des. (1980–2015) **62**, 32–39 (2014). https://doi.org/10.1016/j.matdes.2014.05.001
148. Ramujee, K., PothaRaju, M.: Mechanical properties of geopolymer concrete composites. Mater. Today **4**(2, Part A), 2937–2945 (2017). https://doi.org/10.1016/j.matpr.2017.02.175
149. Collins, F., Sanjayan, J.G.: Early age strength and workability of slag pastes activated by NaOH and Na2CO3. Cem. Concr. Res. **28**(5), 655–664 (1998). https://doi.org/10.1016/S0008-8846(98)00025-8
150. Rangan, B.V.: Fly ash-based geopolymer concrete. Research Report GC 4, Engineering Faculty Curtin University of Technology Perth, Australia (2008)
151. Manjunath, R., Narasimhan, M.C.: An experimental investigation on self-compacting alkali activated slag concrete mixes. J. Build. Eng. **17**, 1–12 (2018). https://doi.org/10.1016/j.jobe.2018.01.009
152. Farhan, N.A., Sheikh, M.N., Hadi, M.N.S.: Investigation of engineering properties of normal and high strength fly ash based geopolymer and alkali-activated slag concrete compared to ordinary Portland cement concrete. Constr. Build. Mater. **196**, 26–42 (2019). https://doi.org/10.1016/j.conbuildmat.2018.11.083
153. Huseien, G.F., Sam, A.R.M., Alyousef, R.: Texture, morphology and strength performance of self-compacting alkali-activated concrete: role of fly ash as GBFS replacement. Constr. Build. Mater. **270**, 121368 (2021). https://doi.org/10.1016/j.conbuildmat.2020.121368
154. ACI 318-08.: Building Code Requirements for Structural Concrete and Commentary. American Concrete Institute (2014)
155. Al-Majidi, M.H., Lampropoulos, A., Cundy, A., Meikle, S.: Development of geopolymer mortar under ambient temperature for in situ applications. Constr. Build. Mater. **120**, 198–211 (2016). https://doi.org/10.1016/j.conbuildmat.2016.05.085
156. Matalkah, F., Ababneh, A., Aqel, R.: Effects of nanomaterials on mechanical properties, durability characteristics and microstructural features of alkali-activated binders: a comprehensive review. Constr. Build. Mater. **336**, 127545 (2022). https://doi.org/10.1016/j.conbuildmat.2022.127545
157. Adak, D., Sarkar, M., Mandal, S.: Effect of nano-silica on strength and durability of fly ash based geopolymer mortar. Constr. Build. Mater. **70**, 453–459 (2014). https://doi.org/10.1016/j.conbuildmat.2014.07.093
158. Younus, S.J., Mosaberpanah, M.A., Alzeebaree, R.: The performance of alkali-activated self-compacting concrete with and without nano-alumina. Sustainability **15**(3), 2811 (2023)
159. Sajjad, U., Sheikh, M.N., Hadi, M.N.S.: Incorporation of graphene in slag-fly ash-based alkali-activated concrete. Constr. Build. Mater. **322**, 126417 (2022). https://doi.org/10.1016/j.conbuildmat.2022.126417
160. Cui, Y., Gao, K., Zhang, P.: Experimental and statistical study on mechanical characteristics of geopolymer concrete (2020)
161. Kar, A., Ray, I., Unnikrishnan, A., Halabe, U.B.: Prediction models for compressive strength of concrete with alkali-activated binders. Comput. Concr. **17**(4) (2016). https://doi.org/10.12989/cac.2016.17.4.523
162. Kar, A.: Characterizations of concretes with alkali-activated binder and correlating their properties from micro- to specimen level. Ph.D. thesis, Department of Civil and Environmental Engineering, West Virginia University, WV, USA (2013). https://doi.org/10.33915/etd.165
163. ASTM C469/C469 M-22.: Standard test method for static modulus of elasticity and poisson's ratio of concrete in compression (2022)
164. ISO 1920-10:2010.: Testing of concrete—Part 10: determination of static modulus of elasticity in compression (2010)
165. AS 1012.17-1997.: Methods of testing concrete Determination of the static chord modulus of elasticity and Poisson's ratio of concrete specimens (2014)

166. BS 1881-121:1983.: Testing concrete Method for determination of static modulus of elasticity in compression (1983)
167. Fernandez-Jimenez, A., Palomo, A., Lopez-Hombrados, C.: Engineering properties of alkali-activated fly ash concrete. ACI Mater. J. **103**(2) (2006). https://doi.org/10.14359/15261
168. Hassan, A., Arif, M., Shariq, M.: Effect of curing condition on the mechanical properties of fly ash-based geopolymer concrete. SN Appl. Sci. **1**(12), 1694 (2019). https://doi.org/10.1007/s42452-019-1774-8
169. Douglas, E., Bilodeau, A., Malhotra, V.M.: Properties and durability of alkali-activated slag concrete. ACI Mater. J. **89**(5) (1992). https://doi.org/10.14359/1832
170. ACI 318-19.: Building Code Requirements for Structural Concrete. American Concrete Institute, MI, USA (2022)
171. ACI 363R-10.: Report on High-Strength Concrete. American Concrete Institute (2010). https://www.concrete.org/Portals/0/Files/PDF/Previews/363R-10web.pdf
172. Aiken, T.A., Kwasny, J., Sha, W., Tong, K.T.: Mechanical and durability properties of alkali-activated fly ash concrete with increasing slag content. Constr. Build. Mater. **301**, 124330 (2021). https://doi.org/10.1016/j.conbuildmat.2021.124330
173. Najimi, M., Ghafoori, N.: Engineering properties of natural pozzolan/slag based alkali-activated concrete. Constr. Build. Mater. **208**, 46–62 (2019). https://doi.org/10.1016/j.conbuildmat.2019.02.107
174. Albitar, M., Visintin, P., Mohamed Ali, M.S., Drechsler, M.: Assessing behaviour of fresh and hardened geopolymer concrete mixed with class-F fly ash. KSCE J. Civ. Eng. **19**(5), 1445–1455 (2015). https://doi.org/10.1007/s12205-014-1254-z
175. Hardjito, D., Rangan, B.V.: Development and properties of low-calcium fly ash-based geopolymer concrete. Research report, Curtin University of Technology, Australia (2005). https://espace.curtin.edu.au/handle/20.500.11937/5594 (Report)
176. Sun, B., Ding, L., Ye, G., De Schutter, G.: Mechanical properties prediction of blast furnace slag and fly ash-based alkali-activated concrete by machine learning methods (2023). https://ssrn.com/abstract=4549275, https://doi.org/10.2139/ssrn.4549275
177. Cong, X., Zhou, W., Elchalakani, M.: Experimental study on the engineering properties of alkali-activated GGBFS/FA concrete and constitutive models for performance prediction. Constr. Build. Mater. **240**, 117977 (2020). https://doi.org/10.1016/j.conbuildmat.2019.117977
178. Kara De Maeijer, P., Ye, G., Li, Z., Ramagiri, K.K., De Schutter, G., Sun, Y., Dehn, F., Kar, A., Yliniemi, J., Ma, Y., Ichimiya, K., Masi, G., Phung, Q.T., Sha, W.: Examining reproducible mix design, fresh and mechanical properties of ground granulated blast furnace slag-based alkali-activated concrete (GGBFS-based AAC): results of an interlaboratory study of RILEM TC 294-MPA. Mater. Struct. **58**, 235 (2025). https://doi.org/10.1617/s11527-025-02754-2
179. Li, Y., Shen, J., Lin, H., Li, Y.: Optimization design for alkali-activated slag-fly ash geopolymer concrete based on artificial intelligence considering compressive strength, cost, and carbon emission. J. Build. Eng. **75**, 106929 (2023). https://doi.org/10.1016/j.jobe.2023.106929